LASER INTERFEROMETER GRAVITATIONAL WAVE OBSERVATORY
- LIGO -
CALIFORNIA INSTITUTE OF TECHNOLOGY
MASSACHUSETTS INSTITUTE OF TECHNOLOGY

Document Type	**LIGO-T960103 - 00-D** July,1996

ASC: Environmental Input to Alignment noise

Gabriela Gonzalez

Distribution of this draft:

Detector group

This is an internal working note
of the LIGO Project.

California Institute of Technology
LIGO Project - MS 51-33
Pasadena CA 91125
Phone (818) 395-2129
Fax (818) 304-9834
E-mail: info@ligo.caltech.edu

Massachusetts Institute of Technology
LIGO Project - MS 20B-145
Cambridge, MA 01239
Phone (617) 253-4824
Fax (617) 253-7014
E-mail: info@ligo.mit.edu

WWW: http://www.ligo.caltech.edu/

1 OVERVIEW

The LIGO interferometer is sensitive to mirrors (mis)alignment in several ways: we need to achieve and maintain a good initial alignment to be able to engage the length locking servos and we need to avoid the misalignments from degrading the sensitivity to gravitational wave signal. The alignment requirements have been written in the ASC DRD (Ref. 1), and they originate in the modeling of the interferometer. The acquisition alignment requirements are 0.5 μrad per angular degree of freedom, and the detection mode alignment requirement is 10 nrad per degree of freedom. Local and interferometric angular controllers are being designed to achieve these requirements, and an important input to this design is the "environmentally produced" angular noise. In other words, we want to know how much the mirrors in the suspensions are going to move in yaw and pitch due to all the reasons we can think of.

We have drawn a schematic diagram that shows this logic for the pitch degree of freedom (Figure 1). [1]

The data will be presented as a "flow", where from the ground up to the mirrors we have at each stage a spectrum that is modified by a transfer function and added to some external input, before exciting the next stage. This is made more clear by the diagram in Figure 1, where each black rectangular box represents an amplitude spectrum and each rounded box a transfer function and/or an external input.This flow diagram is explained in more detail in section 2.

We also built a MATLAB SIMULINK model of the flow diagram, where we can input a time traces for all the environmental noises, model the transfer functions, and get as an output time traces for the mirror motion. We will show the block diagrams and briefly go through the logic used in section 4, then go into details of each block in the following sections. Finally, we present the results obtained for a few different cases, and summarize the conclusions.

2 OVERVIEW II: FLOW DIAGRAM

We show in Figure 1 the flow diagram for pitch angular noise. The coordinate system is a coordinate system with its origin at the "rest position" of the mirror's center of mass, the vertical axis being the "*y*" axis pointing up in the direction of local gravity, and the "z" axis pointing along the optical axis. (The coordinate system convention follows the one described in ASC DRD, section 2.4, Ref. 1). Notice that the coordinate system is defined locally, so the coordinates at each station are rotated with respect to each other, as well as translated and mirrored.

Since the mirrors are curved, a horizontal light beam reflected above or below the center in the mirror will have a tilted return path. Thus, vertical motion of the mirror will be seen as pitch angular noise. This vertical-to-pitch coupling (which adds to the observed angular noise, but is not a physical angular motion of the mirror) is shown at the left of the diagram in Figure 1 , with the last coupling being $y_t / R_m \rightarrow \Theta_{mirror}$.

1. The modeling done in this document is almost exclusively done for the pitch degree of freedom because we think it is going to be the largest one, but we have included the modeling for yaw in our list of "things to do", in section 11.

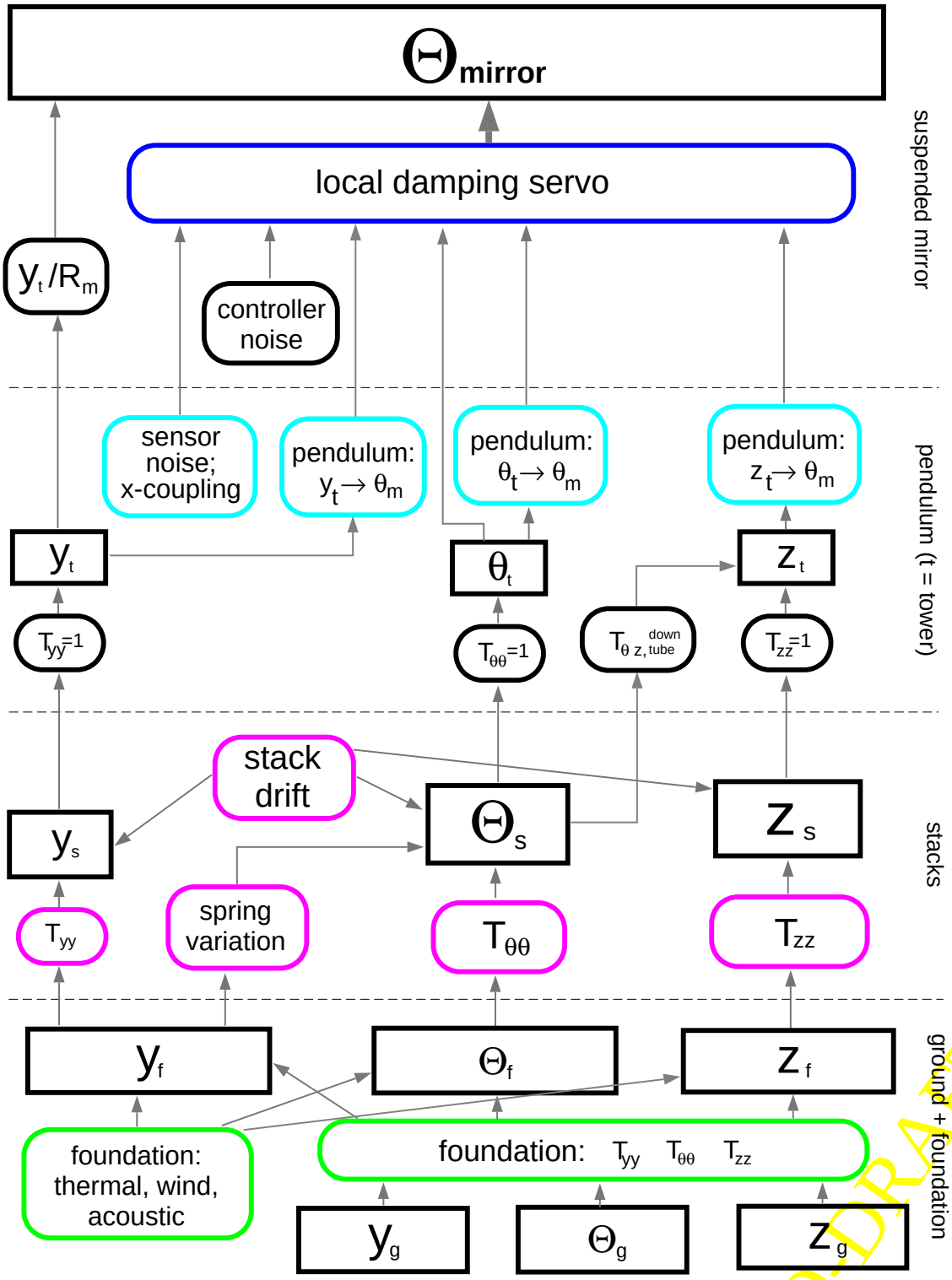

Figure 1: Flow diagram showing the sources of environmental noise converted into angular (pitch) noise of the mirror suspension.

At the very bottom of the diagram in Figure 1, we have the ground motion: we will need to know vertical (y_g) and horizontal (z_g) displacements, as well as ground tilts (θ_g). The building foundations will transfer the ground motion with some transfer functions, and will add its own response to thermal and acoustic excitations, producing some net displacement and tilt of the building floor, y_f, z_f, θ_f. The seismic isolation stacks sit on this floor, and transmit the floor motion with (well designed, non trivial!) transfer functions. The stacks will have cross couplings (that we neglected in the building foundations transfer functions): for example, variations in the spring properties will couple vertical motion to pitch and horizontal motion to yaw. The stacks will also "drift" in position and orientation.

The suspension towers will sit (or "hang") from the last stack stage, and although in principle they have mechanical resonances and thus they modify the stacks motion through their own transfer functions, we will consider those transfer functions to be unity at the frequencies of (our) interest. What we actually need is the motion of the suspension points: the angles will be essentially the angular motions of the stacks, but the displacement of the suspension points will depend on the position of the suspension tower with respect to the stacks. In the BSC, for example, where the suspension tower is attached to a 1-m long "downtube", a pitch angle of the stacks will cause a displacement of the suspension tower. If the tower is not at the center of the optical table, yaw angles will also couple into displacements.

The tower motion excites the pendulum pitch in several ways. The horizontal motion of the suspension points excites both the horizontal and the pitch motion of the mirror (as in a classical "physical pendulum"): this is the $z_t \rightarrow \theta_m$ box. If we take into account the wire elasticity, the angular motion of the tower also excites the pendulum pitch, bending the wires at the top: this is the $\theta_t \rightarrow \theta_m$ coupling. If there is an initial imbalance in the mirror balancing, and the line between the wires attachment points does not go through the mirror center of mass, a vertical motion of the tower will produce a torque and excite the pitch motion: this is $y_t \rightarrow \theta_m$.

All the resonances except the vertical one are damped with either local controllers, referencing to the OSEM sensors or to optical levers signals, and/or interferometric angular controllers (wavefront sensors). Each sensing system has its own reference and sensor noise, but they all have the same driver noise, since they act on the mirror through the OSEM coils. The controllers also some sensor/driver "cross couplings" (between length and angle, for example) that may affect the residual motion.

At the end of the process (top of the diagram), we have the mirror angular motion in its local reference frame.

3 OVERVIEW III: MATLAB MODEL

Once we provide each transfer function and noise generator mechanism in the block diagram, we can predict the spectrum of the angular mirror motion. However, when the mechanisms have so many different time scales, it is also very instructive to have a "time domain" model of the system. We were able to do this with the SIMULINK toolboxes in MATLAB. We modeled each

input noise with a measured trace (for seismic input) or a random time series with the appropriate spectrum, and we created a zero-pole function for each transfer function.

For convenience (simulation speeding), we have separated the model in two “blocks”, one involving the transformation of ground noise into stacks motion, and another converting the stacks motion into pendulum motion. In “matlab-speak”, each block is an M-file that produces an S-function to evolve data with time. We use it with inputs taken from data vectors in the work-space (time traces), and use the simulation to store into the workspace the time traces corresponding to motions at different points in the system. The first block, involving ground+building foundations+stacks, is shown in Figure 2 .

We’ll briefly sketch here what each block represents, and then go into more details in the next sections. Each shadowed box in the block diagram represents a vector that is stored in work-space. In particular the main outputs of this block are *stck_til*t and *stck_disp* (stacks tilt and displacement, respectively).

At the ground level, we input time series (or vectors) (t, y_g, z_g): time, vertical ground noise and horizontal ground noise. To obtain the ground tilt, we use the vertical spectrum filtered by a transfer function, obtained assuming that if the ground is moving vertically at a frequency ω with an amplitude $x(\omega)$, with a wave number function $k(\omega)$, then the tilt is going to be $k(\omega)x(\omega)$. Details and references about the models used for this ground tilt calculation can be found in Appendix 1. The result is stored in the vector *gn_tilt.*

For the building transfer function, we assume them to be unity, but we add two external inputs: one due to thermal deformation of the foundations, and another due to the air pressure fluctuations unbalanced by vacuum on one side of the chamber.

The floor motion is then transmitted through the stacks. The stacks have some horizontal-to-horizontal and tilt-to-tilt transfer function, with a shape depending on the springs used: viton, coil or arch (leaf) springs are the ones considered and modeled by Hytec. There will also be a cross coupling transfer function vertical-to-tilt, due for example to spring asymmetries. The stacks also add their own “drift”, added to the transmitted ground motion.

Once this block is run, we have in the workspace time traces for the stack tilt and horizontal displacement. We then invoke another SIMULINK block that will evolve the stack motion into pendulum motion. This block diagram is shown in Figure 3 .

The block needs as inputs vectors *t, stck_disp and stck_tilt* (time and stacks displacement and tilts). These are then inputs that define the suspension point horizontal displacements, and are converted into a tension horizontal force and torque (where the tension is *Mg*), and then converted into pendulum displacement and tilt. The motion is damped by the damping servos (displacement and tilt controllers). Each controller has sensors that measure the difference between pendulum and sensor positions, so they have two inputs. We have also added to the pitch controller sensor and driver noise.

Once this block is run, we have in the workspace, among other vectors, z and θ, time traces of the pendulum displacement and pitch.

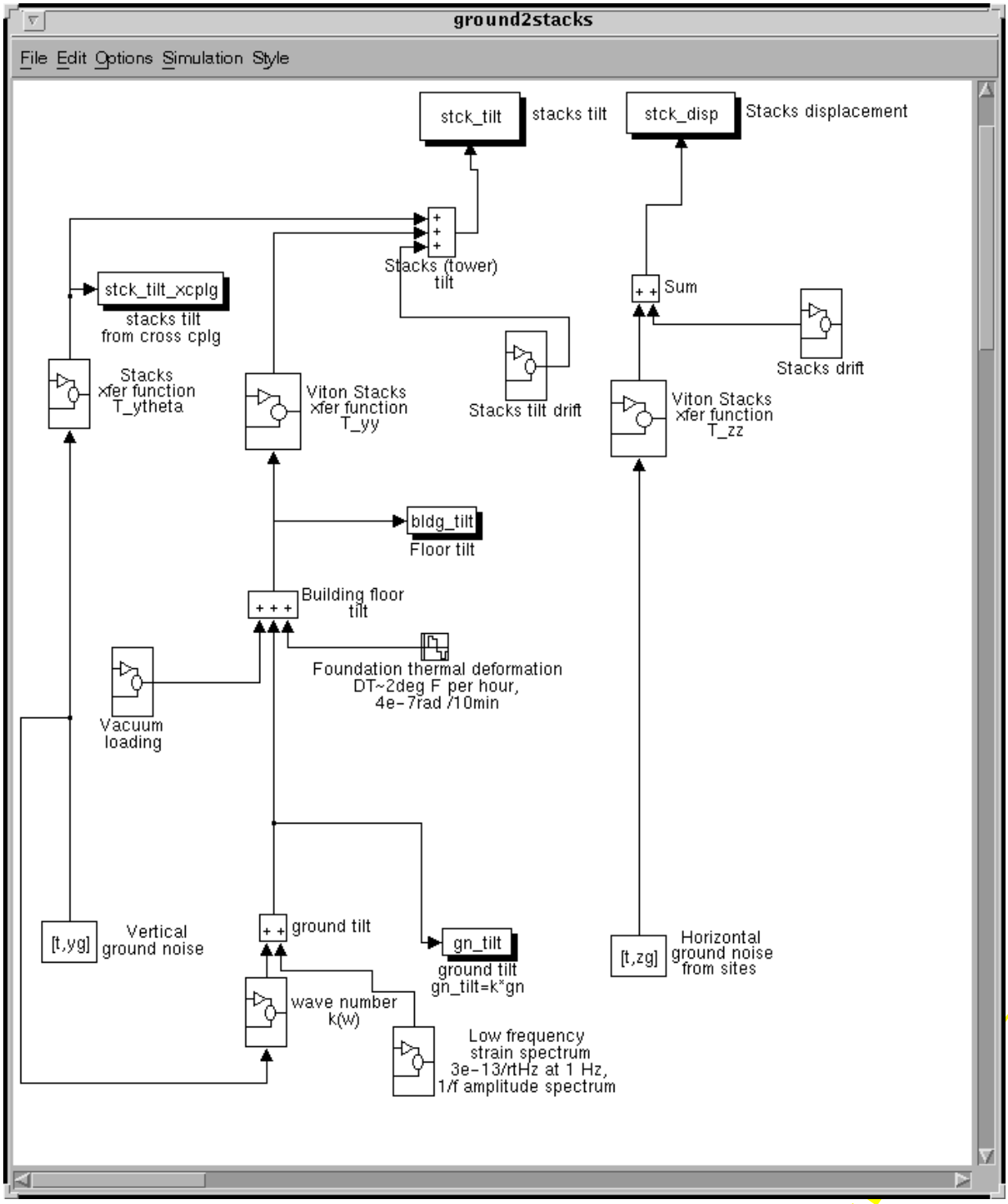

Figure 2: Block diagram for the evolution of ground motion into stack motion.

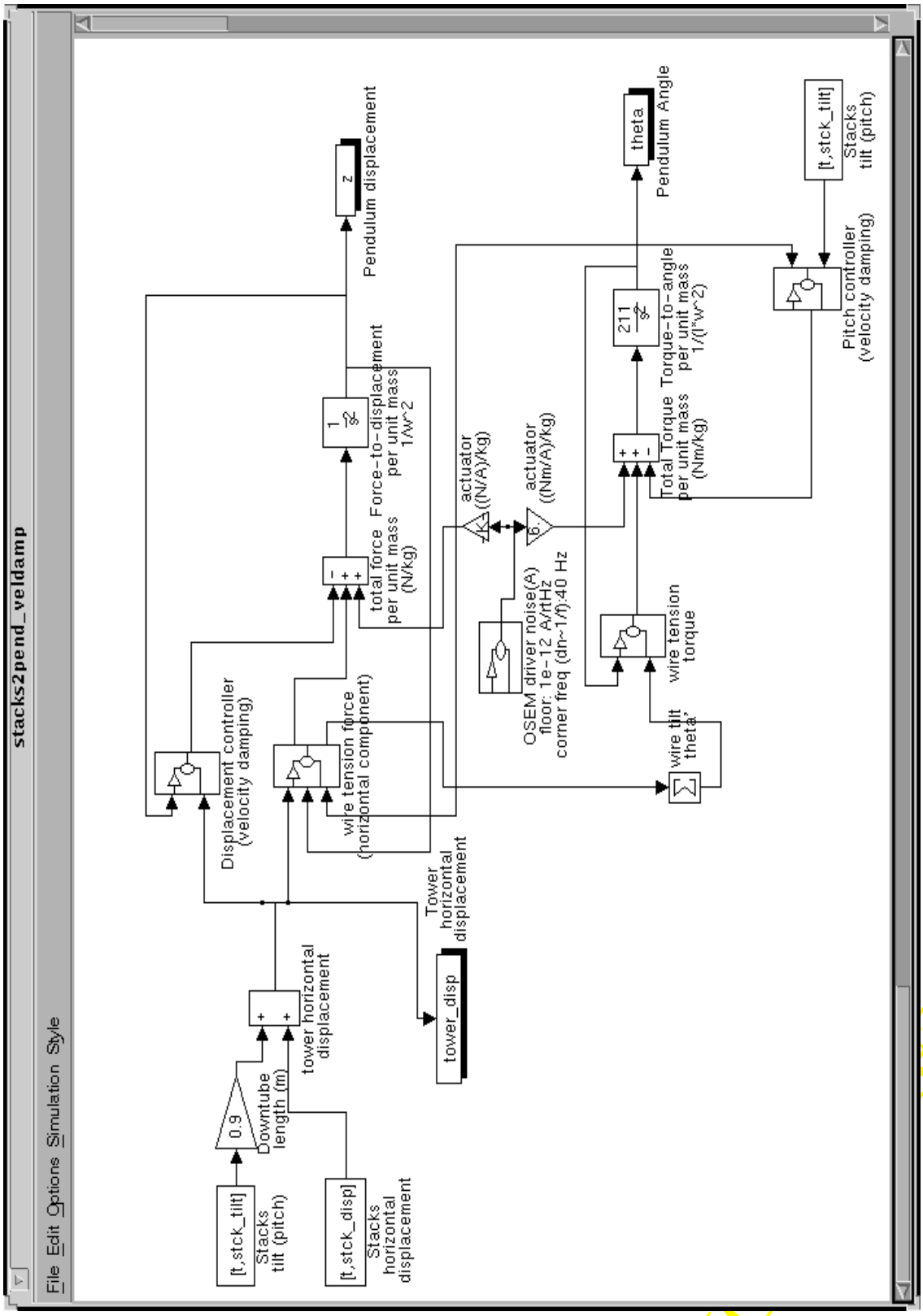

Figure 3: Block diagram for stack motion into pendulum motion.

We will now describe in the following sections the parameters and curves chosen for each block.

4 GROUND NOISE

We use as reference the measurements taken by A. Rohay at the sites (Ref. 2). For the Matlab model, we use time traces for displacement in each direction, in each site, provided also by A. Rohay.

The measured spectra at the sites have been approximated by L. Sievers with straight lines (in log-log coordinates) for frequencies between 0.1 Hz and 100 Hz. As explained in Appendix 1, measurements taken with a seismometer should be corrected subtracting the tilt induced measurements. (These corrections turn out to be important only at frequencies below ~50 mHz.). We show in Figures 4 and 5 the straight lines approximate spectrum, together with the spectra of the considered time traces, corrected by seismometer response. Since the spectra of the time traces follow considerably well the approximation to the average spectrum, we will adopt those time traces as the input data for the modeling that follows.

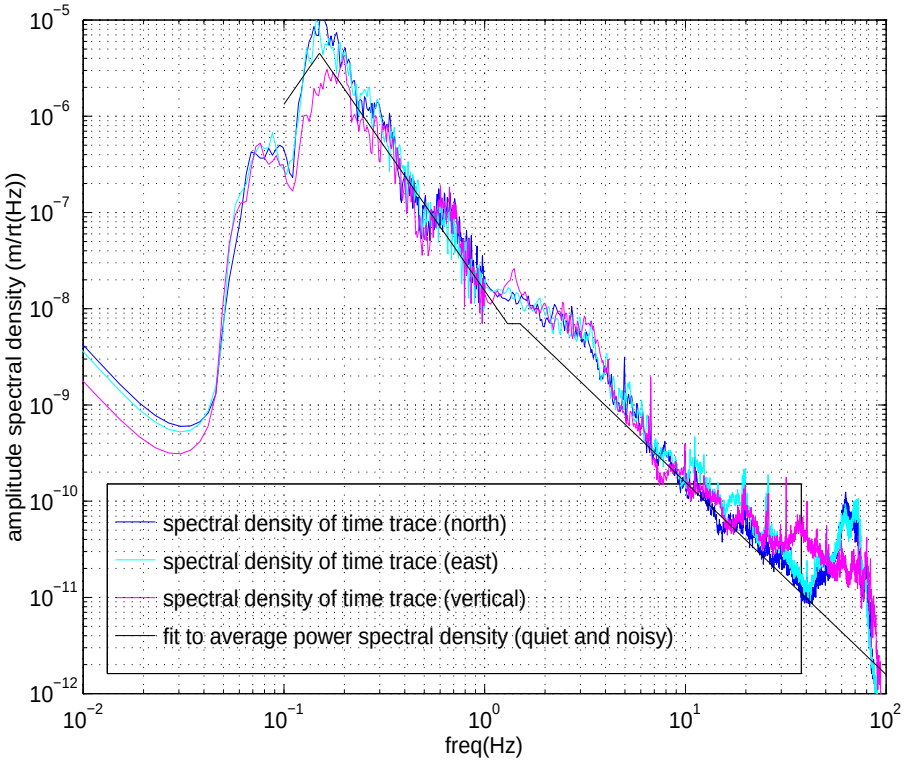

Figure 4: Ground noise (displacement) in Livingston, LA.

Tilts (and shears) are a more delicate matter. Since we do not have direct measurements, we will take the displacement measurements (~x), assume some wave speeds (v~ω/k) and calculate the tilts as $k*x$. Tilts should be deduced from vertical displacements and shears from horizontal displacements. (More details on how the function $k(\omega)$ is modeled and about the validity of this approach can be found in Appendix 1). We show in Figures 6 and 7 the tilts and shears

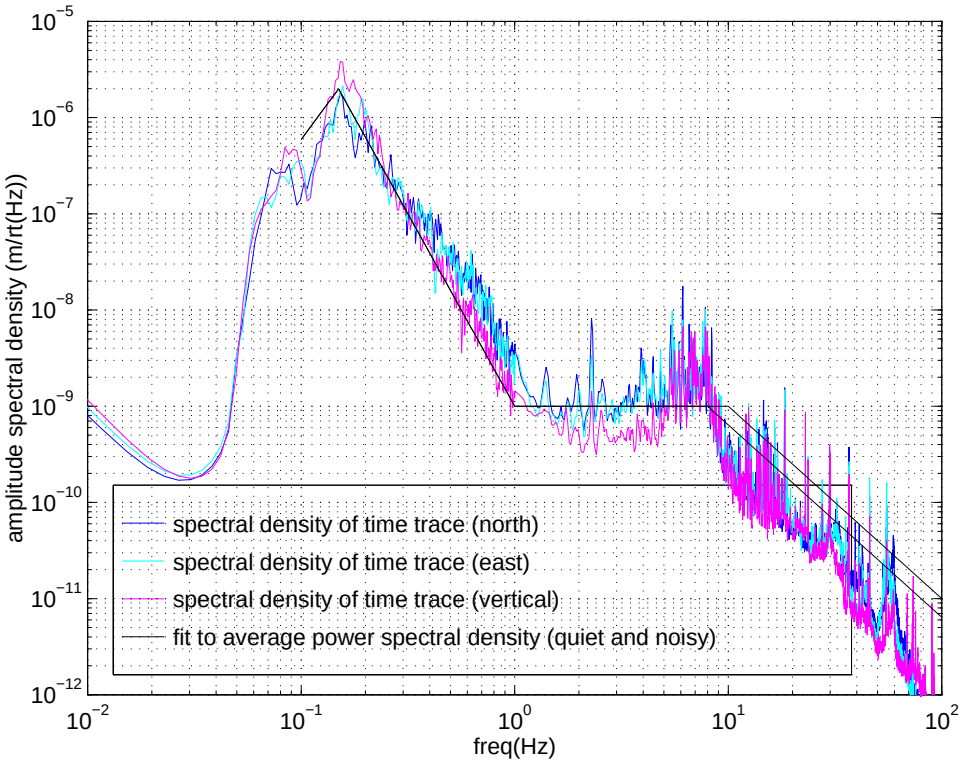

Figure 5: Ground noise (displacement) in Hanford, WA.

obtained with these assumptions. We also included in Figs 6 and 7 upper and lower bounds for strain measurements, taken from Ref. 3 . (These are bounds to the measurements reviewed by the author in Ref. 3).If, as we claim in Appendix 1, tilts and shears are comparable to strains (all ~$k*x$), then our estimate for tilt should be between these bounds, and we see that that is indeed the case, except at the very low frequencies, below 50 mHz, where our estimate is lower than the lower bound, and at the microseismic frequency in LA, where our estimate is higher than the upper bound. However, the spectrum at LA has a large amplitude for the microseismic peak, so it is not surprising that the tilt estimate is also higher than the bounds taken as reference. We have taken for wind velocities a range between 1 and 10 m/s, increasing with frequency.(A. Rohay measured wind speeds in the range 1-10m/s at Hanford, WA), which is probably a reasonable range. The reason for the discrepancy between the calculated ground tilt and the strain lower bound at the frequencies below 50 mHz is likely due to a sharp change of the "real" $k(\omega)$ between the microseismic peak (3 km/s at 0.16 Hz) and the wind-dominated $k(\omega)$, below ~50 mHz: we, however, model $k(\omega)$ with a smooth shape. In order to take a more conservative estimate for ground tilts, we will add noise at the level of the lower bound for strains below 50 mHz.

We will now describe how we used this data in the Matlab modeling.

We first need to input the ground noise: we do this loading the time traces in the workspace. We need vertical noise input (vector *yg*), and horizontal noise input (*zg*). These were taken with a sampling rate of 250 Hz, and they are 600 seconds long. However, the Simulink integration routines have difficulties keeping up with the frequency range between (1/600) Hz and 250 Hz, so we resampled the data with a sampling frequency of 25 Hz. This allows us to create power spectra

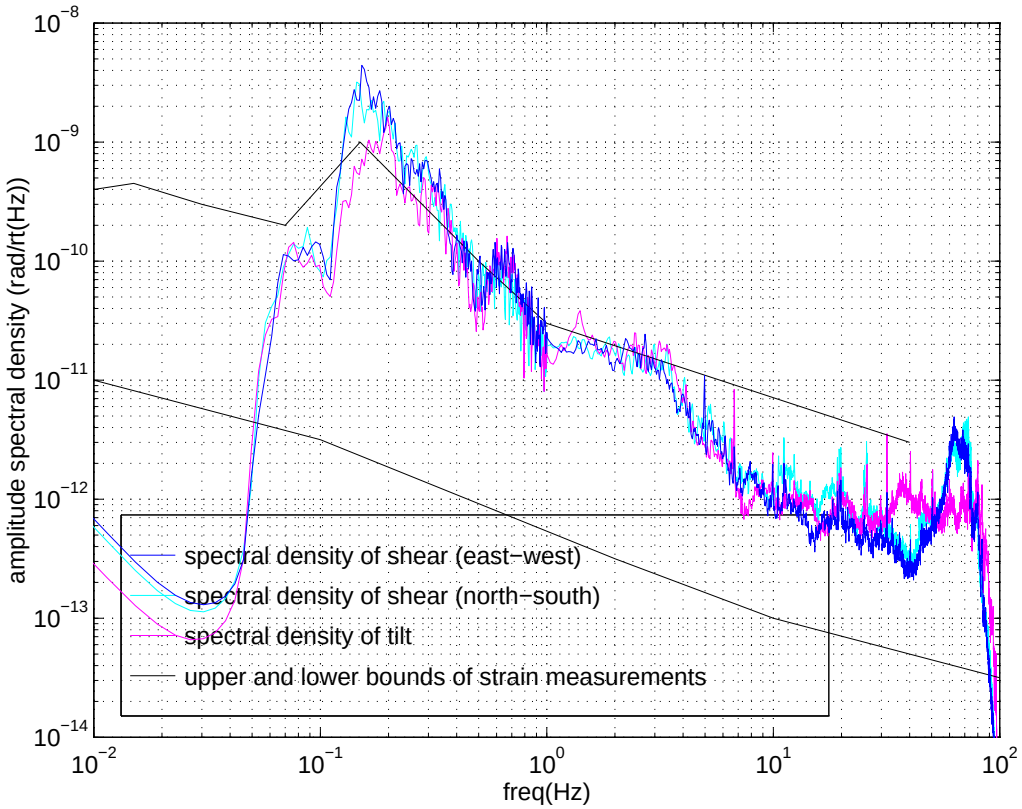

Figure 6: Ground tilts and shears in Livingston, LA

with a frequency range, after windowing and averaging, between the lower frequency resolution of the seismometer (~30 mHz) and 10 Hz. The routine also needs to have defined the constants *dt* (=1/25Hz) for sampling interval, and *T* (=600 sec) for the length of the time record. It also needs a time vector, defined as *t*=[0:*dt:T*], with the same number of elements as the vectors *yg* and *zg*.

We show in Figure 8 the time records used for ground noise in both sites. The data sets for the LA site are 10 minutes long and were taken on Day 303 Hour 19 (Greenwich mean time). This appears to be the noisiest data set in the.1-.25 Hz frequency band which was taken during the measurement period at Livingston. The data sets for the WA site are 10 minutes long taken on Day 345 Hour 04 (Greenwich mean time).

The predominant frequency is, of course, the microseismic peak. It is obvious to the eye, too, how much larger the noise at Louisiana is with respect to the noise at Washington. These traces have a low frequency noise artificially added to the “raw” time traces obtained from A. Rohay. This was done instead of filtering the traces through the inverse of the seismometer frequency response (which what we did in the spectra showed in Figure 4 ,5) to avoid problems with the time integration. The traces added to increase the low frequency spectrum have an added rms about 1000 times smaller than the original trace, so it is not obvious in the time traces, although it makes a difference in their spectra.

In order to calculate the ground tilt, we created a “transfer function“ $k(\omega)$ and implemented it as a “zero-pole box” in Simulink, shown in Figure 9 . Notice that there is added pole at *1/dt* to have a stable numerical inegration.This function roughly follows the few points calculated

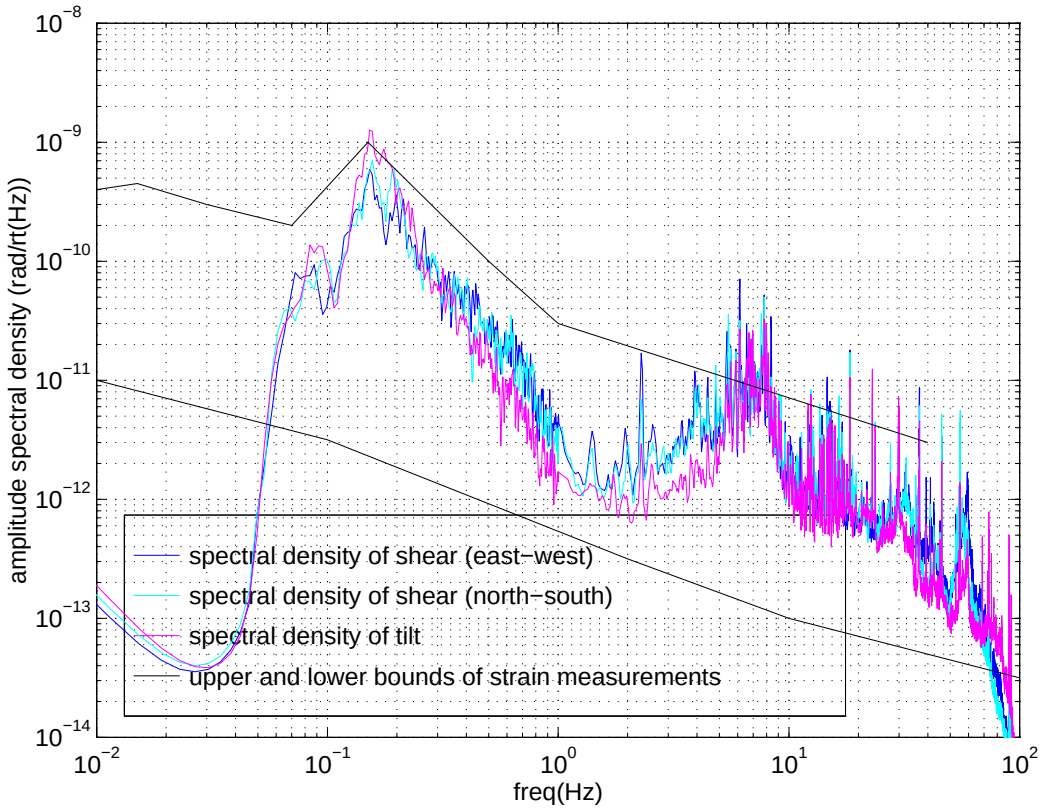

Figure 7: Ground tilts and shears in Hanford, WA.

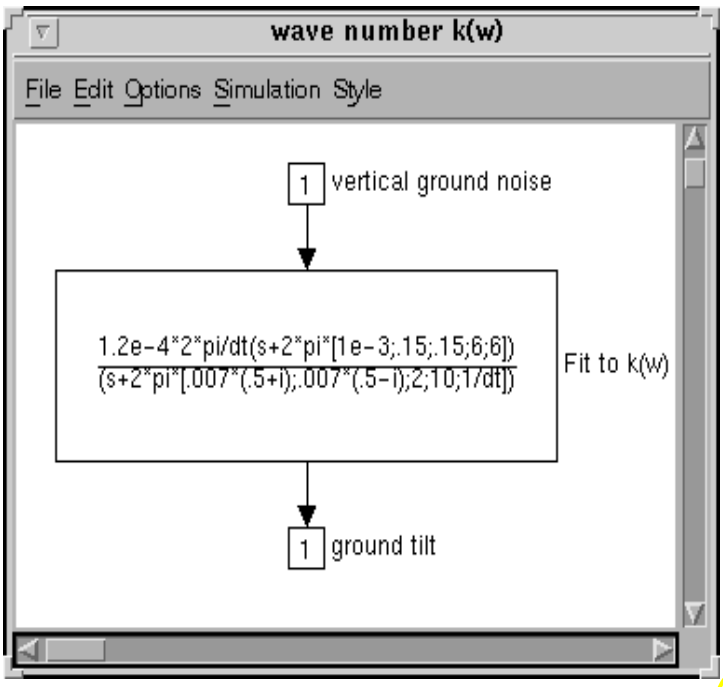

Figure 9: Wave number block (see Figure 2).

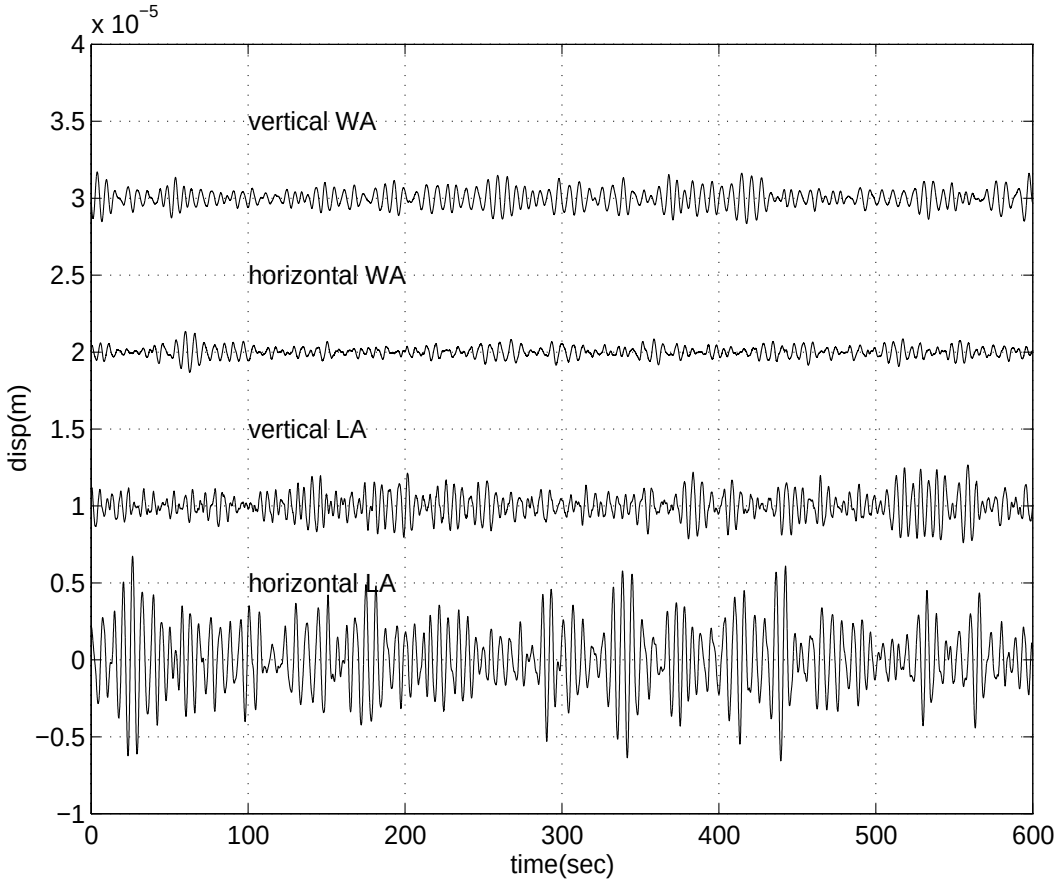

Figure 8: Ground noise traces used in the Matlab model.

taking wind velocities (5-10 m/s) at low frequencies, 3km/s at the microseismic peak and 10 km/s at 5 Hz and above. These few points and the transfer function just described for $k(\omega)$ is shown in Figure 10 .

We add to the calculated ground tilt, a random noise time series with a $1/f$ spectrum, roughly following the lower bound for strain measurements (as shown in the Matlab block diagram in Figure 2).

The resulting ground tilt is then the vertical ground noise integrated through the $k(\omega)$ box, plus the “low frequency” noise. We show in Figure 11 the results for the ground tilt time traces at the two sites. Of course, the spectra are similar to the ones shown in Figure 6 and Figure 7 , except for the added low frequency. Notice that the time traces look very different from the ground displacements, since the microseismic frequency contributes to the tilt spectrum as much as higher frequencies.

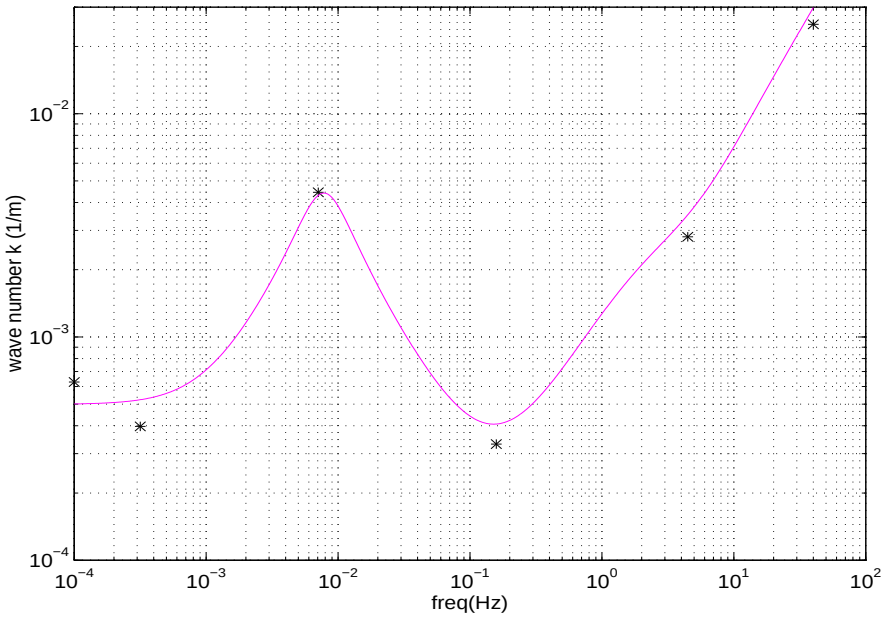

Figure 10: Wave number function used in Matlab model to calculate ground tilts.

5 BUILDING FOUNDATIONS

The next step in the flow consists of the building foundations, responding to the ground noise estimated in the previous section, with added noise due to response to temperature and pressure fluctuations, wind, etc.

We will assume the transfer function from ground to floor motion is unity; but we will add to the ground noise the thermal deformations of the foundation and the tilts due to the vacuum loading.

From the presentation by Parsons in Nov 1995 about the facilities they are building in Hanford (Ref. 4) WA, we take an estimate for the thermal deformation of the slab. They estimate the deformation of the slab (vertical displacement and angle in the small dimension, as a function of distance from the center), over 10 minutes, assuming a temperature change of 2 degrees F at the surface in one hour. They estimate the deformation for different slab thicknesses (18", 36" and 68") and different "small slab dimensions" (90m, 45m and 12m). I'll take my estimates for a 36" foundation, 12m wide slab (narrow LVEA quadrant).The shape of the deformed cross section is a curve 45 µin high at the center, crossing zero at 3.5m, and reaching -80 µin at 5.5m from the center. Therefore, the maximum displacement is 2 microns at 5.5m. For tilts ("rotations" in the Parsons graph), the shape is a linear function from zero to 2m, with a slope ~200 nrad/m, and a linear shape with a shallower slope (~30 nrad/m) from 2 to 5.5 m.

In the Matlab model, we added thermal deformation to the ground tilt in the form of a sine wave with a 1 hr period and amplitude 4.6×10^{-7} radians (see Figure 2). This gives a tilt amplitude

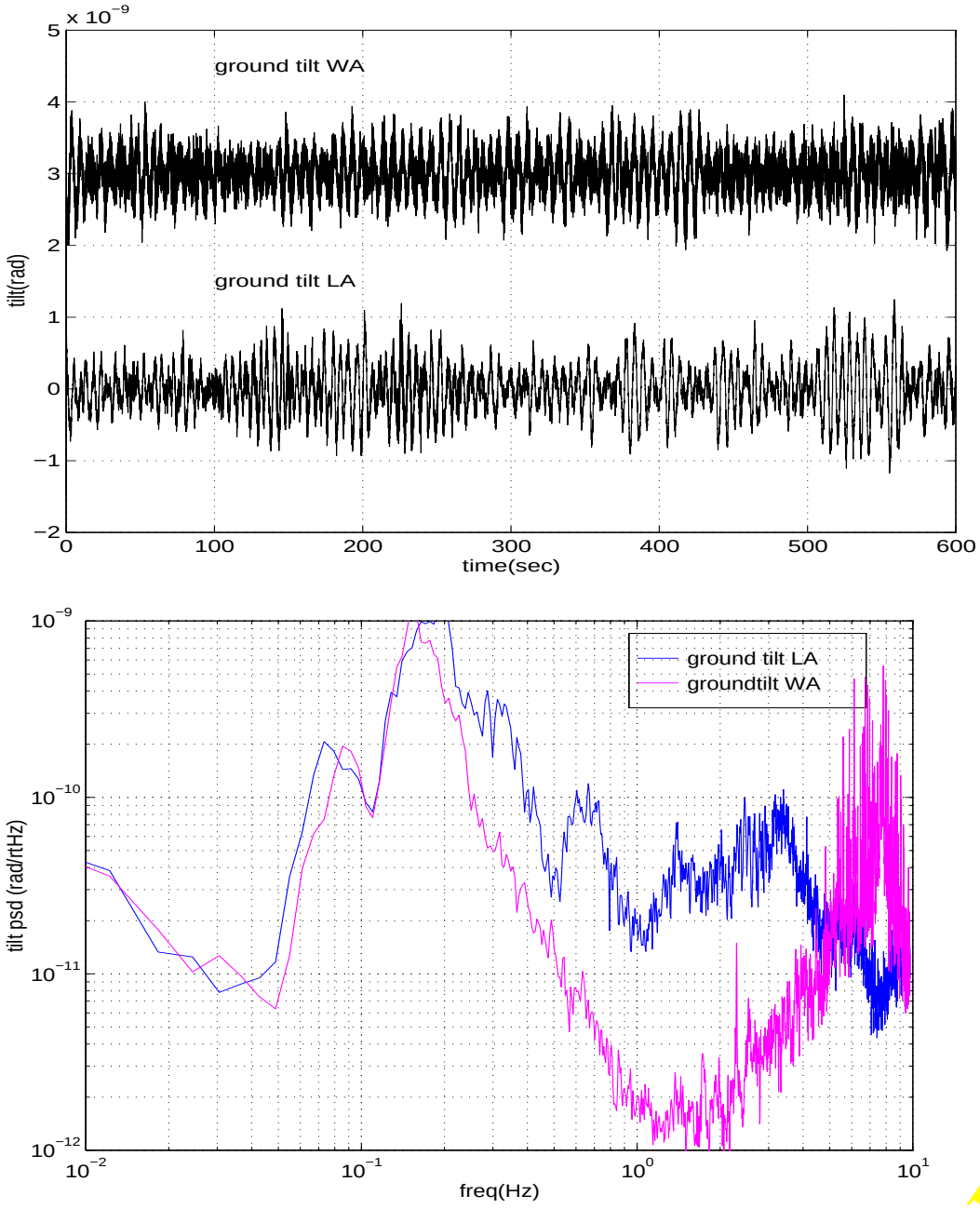

Figure 11: Ground tilt time traces and spectra obtained with the Matlab model.

equal to 4.0 10^{-7} radians at t=10 minutes, which is the estimated tilt at a distance equal to 1.5m from the center of the slab.We choose a random sign for the amplitude, and start at zero phase (i.e., the initial tilt is zero).

The other source of noise that the slab adds to tilts is due to “vacuum loading”. The static load was estimated by Dennis Coyne (Ref. 5) for a 30” foundation as 222 microradians for a change in pressure equal to one atmosphere, at the initial pumpdown. Due to pressure fluctua-

tions, the tilt will also fluctuate. We took from Ref. 6 an measured air pressure spectrum, and scaled it using the estimated static load 222 μrad/atm.

In the Matlab model, we produce a time record with random numbers with unit spectral density, and pass it through a "pole-zero transfer function" that approximates the spectrum in Ref. 6 . We display in Figure 12 the contents of the "Vacuum loading block" (used in the ground to stacks Simulink block shown in Ref. 2).

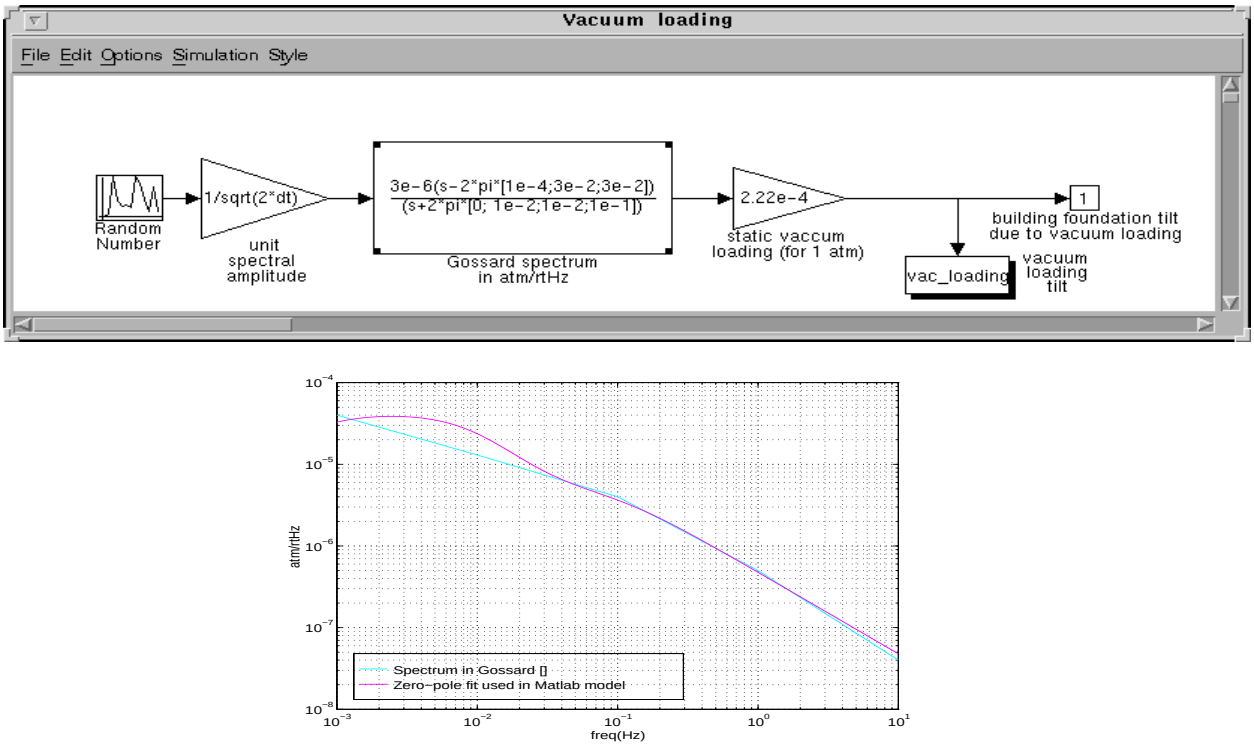

Figure 12: Vacuum loading Simulink blocks and fit to pressure fluctuations in Ref. 6 .

6 STACKS

The stacks have very non trivial transfer functions that provide the seismic isolation above their resonances. Hytec has so far considered three designs: one with viton springs, and two other designs with "leaf" springs and with "coil" springs.

6.1. Horizontal, vertical and tilt transfer functions.

The transfer functions (horizontal-horizontal and vertical-vertical) have been modeled for the Simulink model for viton and leaf spring stacks. Eric Poinslet from Hytec provided us with the complex vectors Hay(ω) (vertical) and Hz(ω) (horizontal) that were obtained from their modeling[1], and we fit the transfer functions with zero-pole blocks in Simulink. We plot the stacks transfer functions and the fits in Ref. 13 .

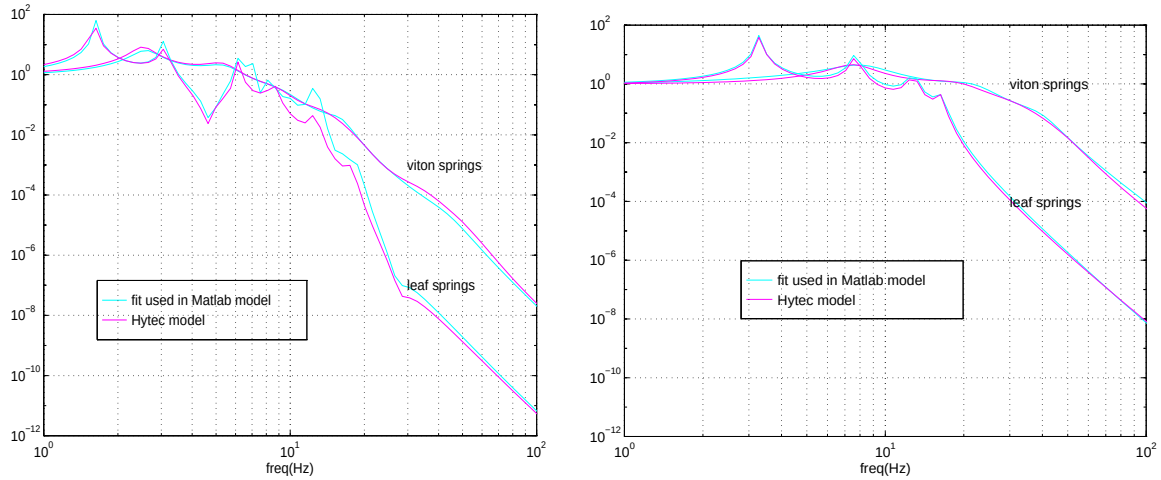

Horizontal transfer functions **Vertical transfer functions**

Figure 13: Stacks transfer functions: viton and leaf springs.

It is obvious from the transfer functions that the resultant noise using different stacks will be very different at low frequencies (below 10 Hz) due to the resonances of the stacks.

We also need the tilt-to-tilt transfer functions. Since we don't have these, we will use the vertical-to-vertical transfer functions.

6.2. Cross couplings: vertical to tilt.

Another transfer functions we need are "cross couplings": vertical to horizontal, horizontal to vertical, horizontal to shears (rotations) and vertical to tilts. There are no estimates yet from Hytec for these cross couplings[1], but we can make an estimate from the analysis done in the stack prototypes. In those, a 5% variation in spring constants was observed, and that variation gave consistent results for cross-couplings (at higher frequencies) when introduced in the FE analysis (Ref. 7). An variation in the springs would make the vertical motion couple into tilts, and the horizontal motion couple into shear. In a simple model with a single stage stack with two springs differing by Δk, the tilt to ground motion transfer function is

$$\frac{\theta}{y_g} = \frac{1}{l}\frac{\Delta k}{k}\frac{(f/f_p)^2}{(1-(f/f_p)^2)(1-(f/f_r)^2)}$$

where $f_p = \frac{1}{2\pi}\sqrt{\frac{k}{M}}$ and $f_r = \frac{1}{2\pi}\sqrt{\frac{k}{(J/l^2)}}$ are the resonant frequencies, and M is the stack mass, J is its moment of inertia, and l is the distance of the springs to the center of the stack. At

1. E. Poinslet has just provided us with mode data from their modeling that we did not have time to include in the modeling for the data presented in this document.

low frequencies, the transfer function decreases with the square of frequency like $\frac{l\theta}{y_g} = \frac{\Delta k}{k}\frac{\omega^2 M}{2k}$.

For a two stages stack, the coupling at low frequencies is $\frac{l\theta}{y_g} = \frac{(\Delta k_1 \pm \Delta k_2)}{k}\frac{\omega^2 M}{2k}$ (the sign depending on whether the spring differences cancel each other or add to each other) The shape of the transfer function for a multilayer stack has a f^2 slope at low frequencies and a f^{2n} at high frequencies (above resonances). As we saw in the 1-layer stack, the resonances are at not only at the "vertical" resonances but also at the 'tilt" frequencies, depending on the moments of inertia of the stack elements. Since we don't have any information on these, we assumed a "flat" transfer function between 1 and 10 Hz, and slopes f^2 at low frequencies and f^8 at high frequencies.

In Ref. 14 we show the block used in the Matlab model, that follows the description given in the previous paragraph.

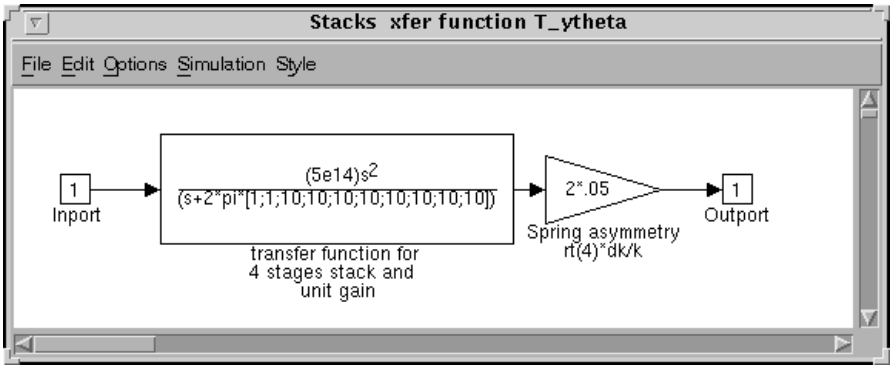

Figure 14: Matlab block for vertical-to-tilt stack transfer function.

6.3. Stack drifts.

The stacks will drift, producing both a displacement and an angle drift that have to be added to the filtered ground noise. Based on observations in the 40m stacks and in the stack prototype, there were requirements written up in the SEI DRD (Ref. 8): for horizontal drift, a constant velocity equal to 6×10^{-10} m/s, and for tilt, a constant velocity equal to 8×10^{-11} rad/s. Notice that these are conservative assumptions, since drift rates are assumed to decrease logarithmically with time.

7 GROUND TO STACKS: RESULTS.

We plot in Figure 15 the tilts power spectral densities obtained for viton stacks with LA ground noise.

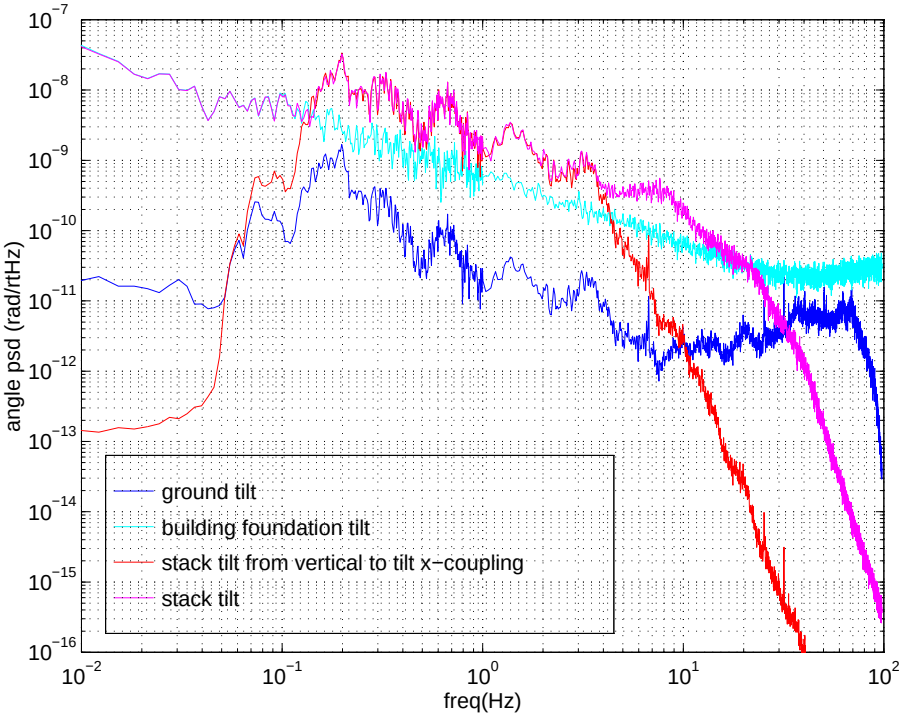

Figure 15: Tilts at different points, from ground to stacks, with viton stacks and Livingston ground noise.

The stacks tilt is mostly due to the building tilt filtered by the stacks, only superseded by the vertical-to-tilt cross coupling due to spring asymmetries between 0.1 Hz and 5 Hz. The building tilt, in turn, is almost exclusively due to air pressure fluctuations: the ground tilt only comes close to that at the microseismic peak. These features are generic to the different stacks and the two sites, so we only show them for viton stacks and Louisiana ground noise.

The time series for tilts show the effect of drifts, which does not add much except to the lowest frequency bins in the spectral densities. We plot the tilt time traces again only for Louisiana ground noise and for viton stacks, in Figure 16 .

We show in Figure 17 the results obtained with the Matlab model for Hanford and Livingston, for viton and leaf spring stacks, using the first Simulink block shown in Figure 2 for the noise propagation from ground to stacks. Notice that the leaf spring stacks results are scaled down for clarity.

8 PENDULUMS

So far, we have an estimate of the stacks (or, optical platform) motion: horizontal translation and tilts.

The stacks translations and tilts produce equal translations and tilts of the suspension tower, that is to say, we will assume a unity transfer function from stacks to suspensions towers. In the BSC chamber, the suspension towers are bolted to the optics plate that is attached to the stacks

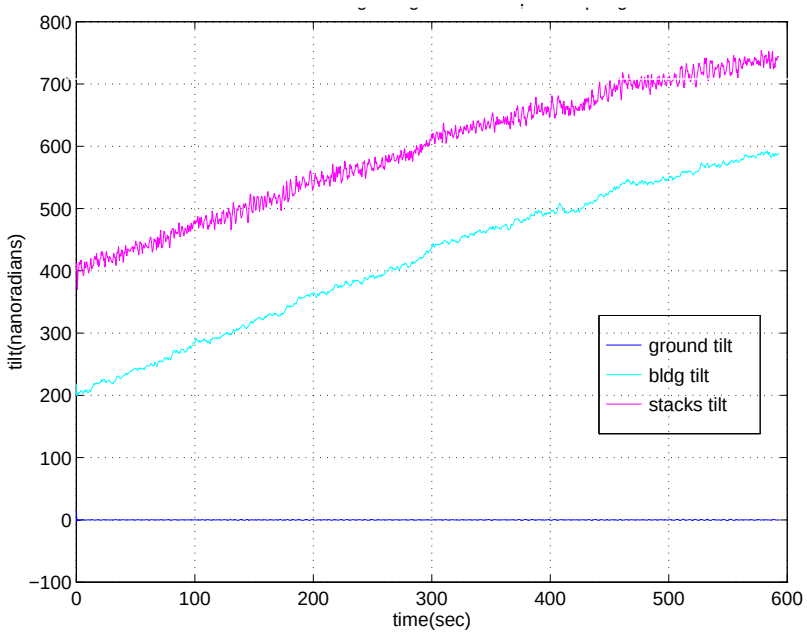

Figure 16: Tilt time traces, from ground to stacks, for viton stacks and Livingston ground noise.

through a “downtube” 0.90 m long. Tilts of the stacks will then produce translations of the suspension tower, through the lever arm of the downtube. These translations are added to the stacks translations as shown in Figure 3 . We show the comparison of these two contributions in Figure 18 . Notice that the stack displacement determines the integrated rms displacement of the suspension tower and its spectrum at frequencies below a few Hz, but it is the stack tilt the one that determines the “drift rate” and spectrum below few tens of mHz, as well as the high frequency spectrum. The assumptions in the calculation of stack displacement are rather solid (ground motion+stack transmission). The models that determine the stack tilt spectrum at high frequencies are the building foundations tilt due to air pressure fluctuations transmitted through vacuum loading, and the tilt-to-tilt stack transmission, assumed similar to vertical-to-vertical. These assumptions should be looked at more carefully.

Motion of the suspension tower will couple into pendulum motion in different ways. If the suspension does not have any asymmetries (i.e., wire take offs are at symmetric positions with respect to the center of mass, etc.), then pendulum pitch angle θ and longitudinal motion z are excited by the longitudinal motion of the suspension, while the pendulum yaw angle ϕ is excited by yaw motion (rotation) of the suspension tower. If there are small asymmetries in the suspension, then there are “cross couplings” that add to the mentioned “straight” couplings. These are described in more detail in Ref. 11 .

8.1. Pitch

Stack (or optical platform) tilts around the x-axis are going to couple to pendulum motion only through the bending of the wire at the top; using a model for a pendulum including the elasticity equations of motion, we concluded that a tilt produces the same effect as a translation in the

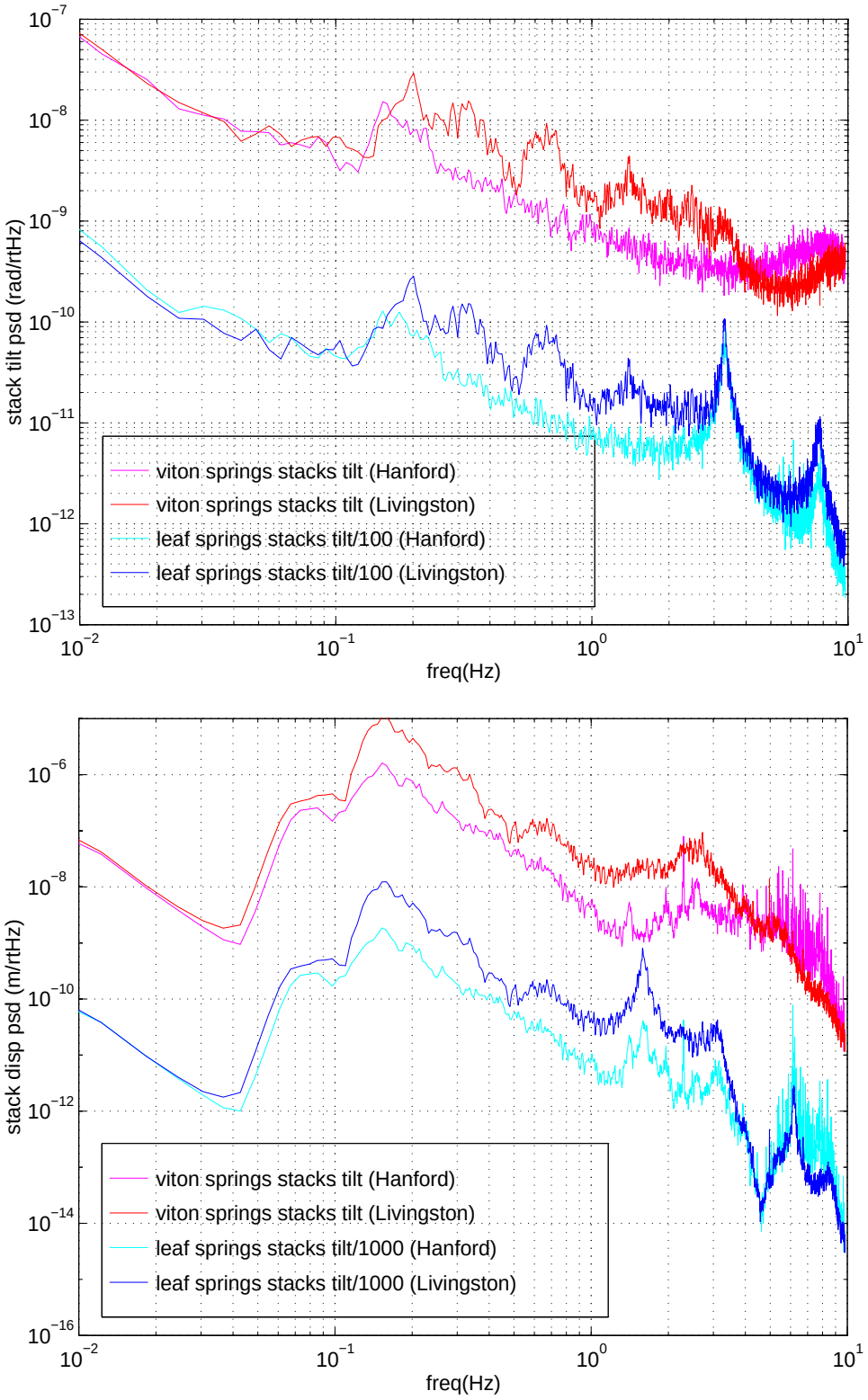

Figure 17: Stacks tilts and displacements obtained with the "ground to stacks" Matlab model.

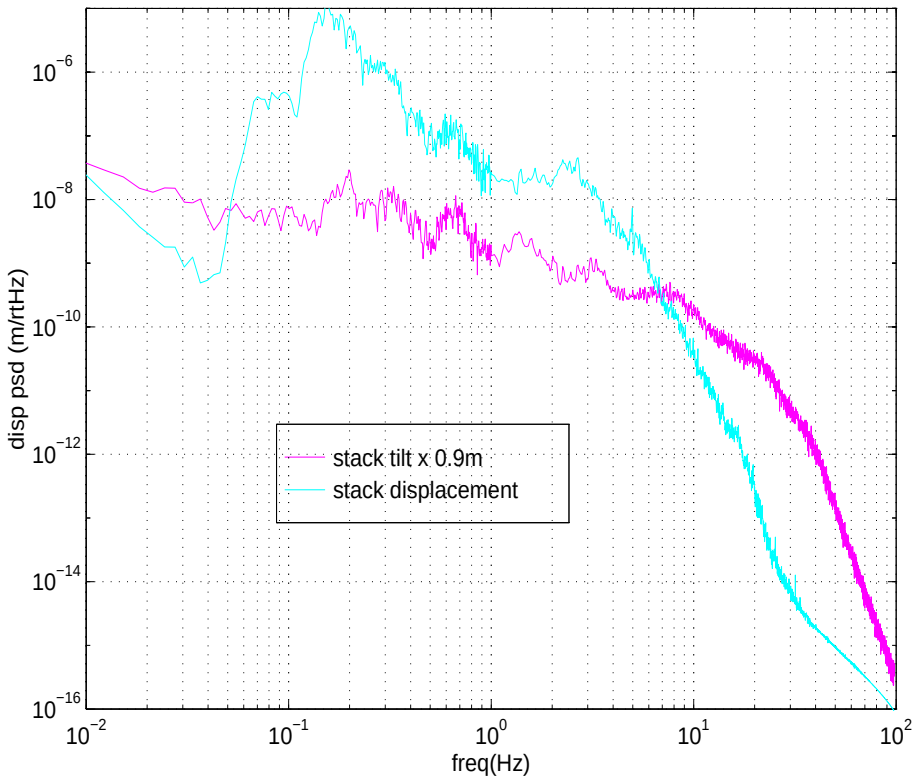

Figure 18: Contributions of stacks tilts and displacements to the suspension tower displacement.

appropriate direction scaled by an "elastic length" (the distance over which the wire bends), given by $\sqrt{EI/T}$, where E is the Young's modulus, I is the area moment of inertia, and T is the tension. This distance is of the order of fractions of mm for the LIGO wires (it is the ratio of pendulum length to this distance what gives the gain factor in Qs from the material Q to the pendulum Q). Therefore, we have a "coupling factor" of ~10^{-3} m/rad (probably smaller than that). However, the ratio of stacks displacements to tilts is always more than 1 m/rad (see Figure 17), therefore tilts are going to excite the pendulum motion much less than displacements. Thus, we will not consider tilt couplings into the pendulum (although tilts will show up in the OSEM sensors motion, that we will consider later).

The motion of the pendulum in θ is coupled to the longitudinal ground motion Z, with a transfer function

$$\frac{\theta}{Z} = \frac{\omega^2/g}{(1-\omega^2/\omega_p^2)(1-\omega^2/\omega_\theta^2)}$$

showing resonances at the pendulum frequency (ω_p)and the angular pitch frequency(ω_θ). Notice that both below the resonances, the transfer function is proportional to ω^2, and above the reso-

nances, it is proportional to ω^{-2}, so the pendulum acts as an isolator both for high frequencies and low frequencies.

However, the pendulum is normally not free to swing, but we have local damping servos, or alignment servos working on them too. The solution for the pendulum motion in pitch is coupled to the longitudinal motion *z,* and the equations, their solutions and the Matlab block model corresponding to the system were described by S. Kawamura in Ref. 8 .

The equations for z and θ, assuming that we apply damping forces in both degrees of freedom, are:

$$-M\omega^2 z = -\frac{Mg(z - Z - h\theta)}{L - h} - K_x(\omega)z$$
$$-J_x\omega^2\theta = \frac{Mgh(z - Z - L\theta)}{L - h} - K_\theta(\omega)\theta$$

where M is the suspension mass, J is the pendulum moment of inertia, h is the pitch distance and L is the pendulum length.

The first term on the right hand side of the equations is the tension force (or torque), while the second term is the damping force. For velocity (viscous) damping, $K_{z,\theta}(\omega) \propto \omega$, and this is the function used in the local controllers (with a a Chebyschev filter used to cut down the noise at high frequencies).

The equations shown above are implemented in the Matlab model as shown in Fig. 3. (The terms have all been scaled by the mass). The source term *Z*, which is the longitudinal motion of the suspension tower, is made up of two added terms, as we explained earlier: the stack displacement and the stack tilt times the downtube length. (These are shown in the upper left of the block diagram in Fig. 3). The source *Z*, the pendulum motion *z* and the pendulum pitch angle θ are the inputs to the “wire tension force” block, shown in Figure 19 . The combination $(z - Z - h\theta)/(L - h)$ is the wire angle with respect to vertical, called θ' in Ref. 8 .

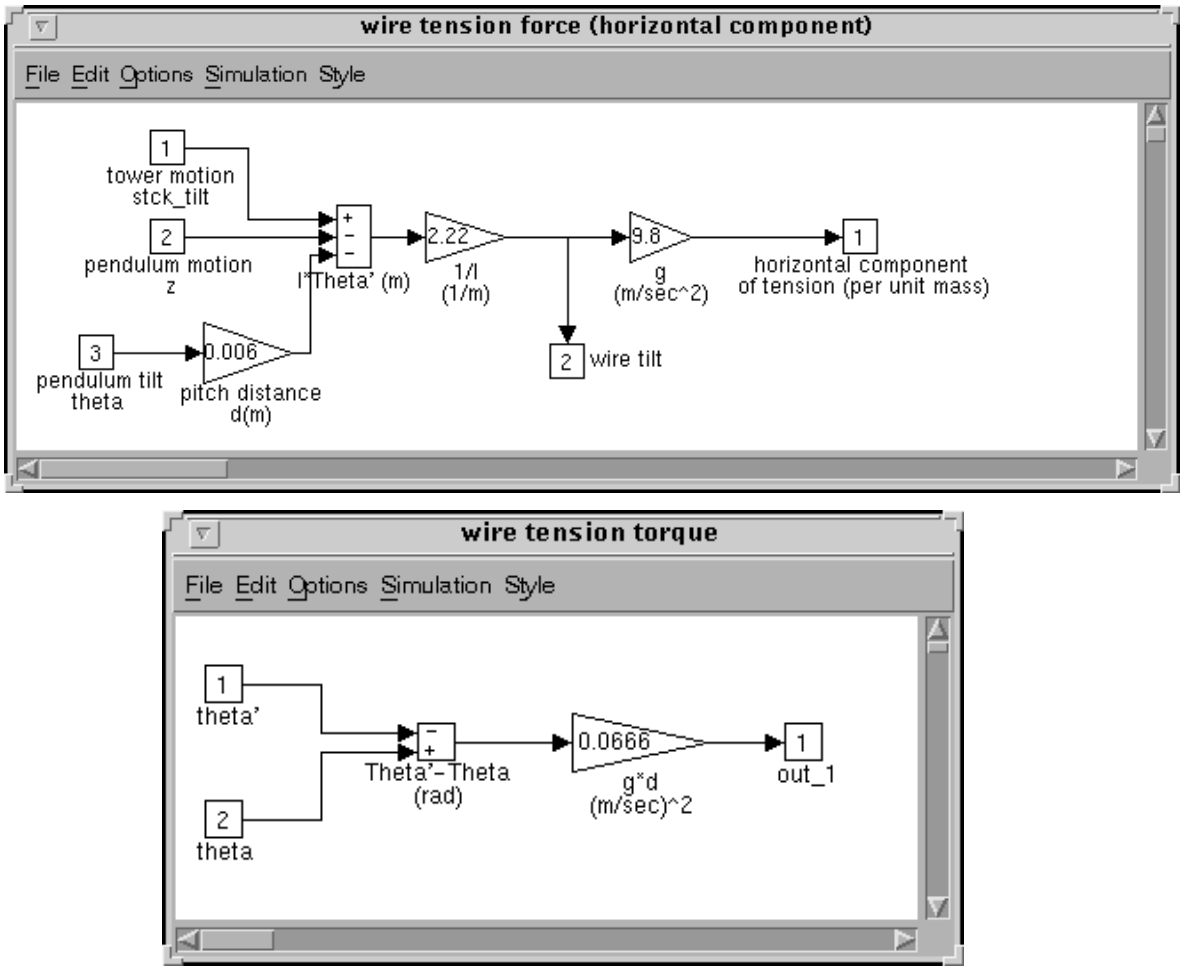

Figure 19: Wire tension force and torque blocks (refer to Fig. 3)

The source term for the θ equation is the same as for the z equation, multiplied by the tension "lever arm" h, minus $Mgh\theta$:

$$\frac{Mgh(z - Z - L\theta)}{L - h} = -Mgh\theta + \frac{Mgh(z - Z - h\theta)}{L - h} = Mgh(\theta' - \theta)$$

Thus, the "tension torque block", has two inputs: the wire angle θ', and the pitch angle θ, multiplied by gh (since we are calculating forces and torques per unit mass), as shown in Figure 19 .

8.2. Yaw

The motion of the pendulum in ϕ is more straightforward. Assume the suspension tower moves in yaw by Φ, the transfer function is simply

$$\frac{\phi}{\Phi} = \frac{1}{1 - \omega^2/\omega_\phi^2}$$

where ω_ϕ is the yaw resonance. If, as argued in Appendix 1, ground yaws are similar to ground tilts (and to ground strains), and if the stacks yaw-to-yaw transfer functions are not very different from others, then the pendulum yaw motion should be much smaller than pitch.

9 CONTROL/DAMPING SERVOS

The pendulums are going to be controlled in angle by either a local damping servo, or another angular control servo, such as wavefront sensing. Either way, the forces are going to be applied through the OSEM coils, which have some associated driver noise (at a minimum, the Johnson noise of the resistors in the last stage). We considered three designs for the pitch controllers: a simple velocity damping servo, described in Ref. 8 ; a “modified” velocity damping with some added gain at low frequencies (used to reduce the overall pitch rms); and a “wavefront servo”, described in the ASC Conceptual Design (Ref. 1).

The driver noise (common to all the damping schemes) is estimated in the SUS PD Ref. 8 as 10^{-12} Amp$/\sqrt{\text{Hz}}$ at 40 Hz. We assume it has a $1/f$ spectrum with a corner frequency ar 40 Hz, and multiply by the appropriate factor in the length and pitch controller to convert it into forces and torques.The “driver noise” block in the Matlab model is shown in Figure 20 : it generates a white noise time record, and filters it through a transfer function that has the shape and magnitude of the driver noise. We also show the curve fitted with the zero pole function shown in the block. (A $1/f$ power law is not easily fitted with poles and zeros, but we tried to be conservative in the fitting).

9.1. Velocity damping servo

The basic velocity damping servo (for pitch) is the one is described in Ref. 8 . The inputs are the pendulum angle, the OSEMS angle (equal to the suspension tower tilt, equal in turn to the stacks tilt) and the sensors noise. The output is a torque that gets added to the tension torque and the drivers noise. We show the Matlab block diagram in Figure 21 . The displacement controller is identical except for the gain stage being 4 instead of 0.05.

The sensor noise in this servo is also taken from the SUS PD (Ref. 8), and from Ref. 10 : the description of the noise is “10^{-10} m$/\sqrt{\text{Hz}}$ (per OSEM) at 100 Hz; below 50 Hz, the spectrum rises approximately as $f^{-1/2}$, while below 1 Hz the spectrum seems to approach $1/f$.[1] We show in Figure 22 .the Matlab model we use to approximate these estimates, together with the curve that we used to fit the sensor noise. The sensor noise per OSEM is then added in quadrature

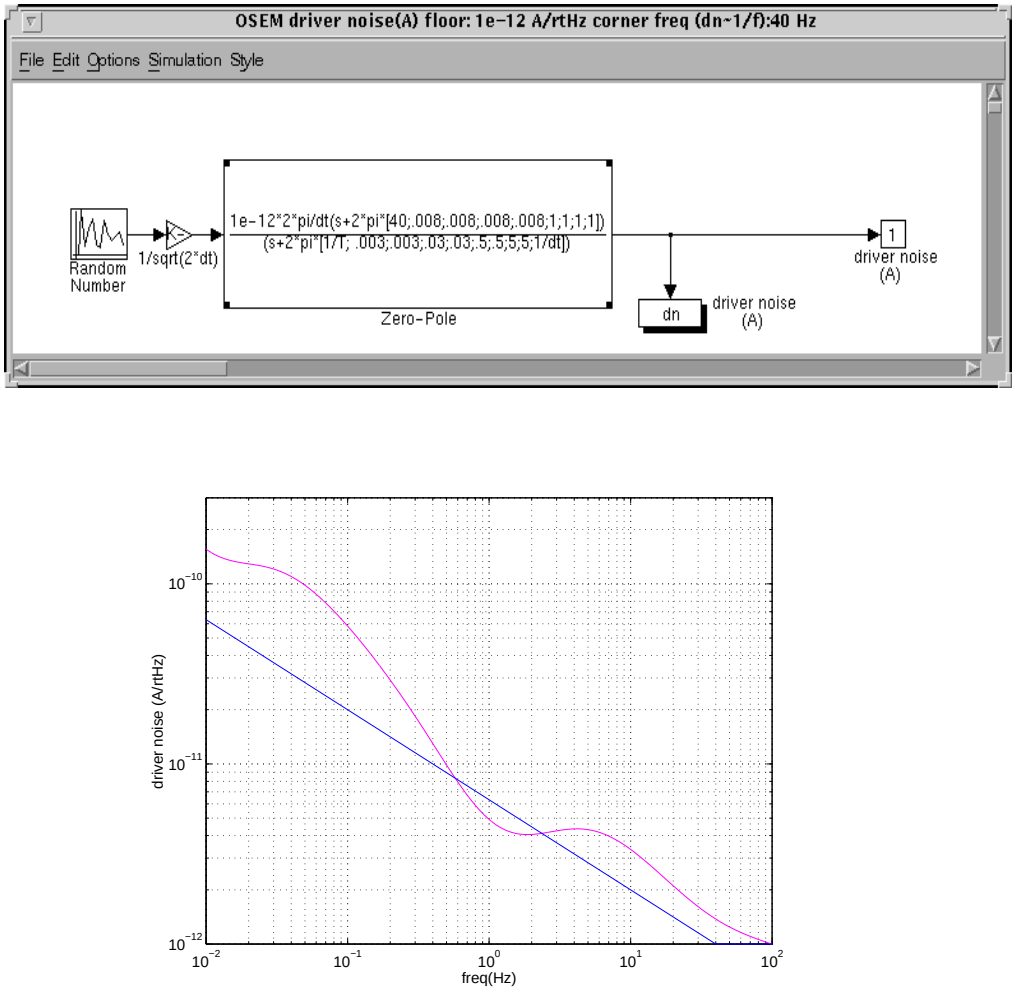

Figure 20: OSEM driver noise: block diagram, estimated and zero-pole fit.

for the 4 sensors, and converted into angle using the lever arm of the sensors, 8.1 cm (for LOS). We show in Figure 23 the results for residual pendulum pitch angle obtained for the Louisiana ground noise, viton spring stacks and using this servo. The results are different for both sites and for different stacks, but the qualitative features are the same:

- the driver noise contribution, calculated as the driver noise as torque in Nm, divided by $J\omega_\theta^2$, (J=moment of inertia, ω_θ=pitch frequency), is orders of magnitude below other contributions. Of course, the driver noise has to be looked as a possible noise contributor in the gw band, but at low frequencies it is negligible.
- The suspension tower tilt (same as stacks tilt), is below the sensor noise, so the controller tilt reference is given by sensor noise and not by its own motion.
- The pendulum driving source in pitch is the suspension tower displacement, not shown in Figure 23 . We plot in Figure 24 the motion of a free pendulum excited by the tower displace-

1. Recent measurements in the new suspension in the 40m prototype indicate that the sensor noise might be up to 10 times larger than the estimate used here.

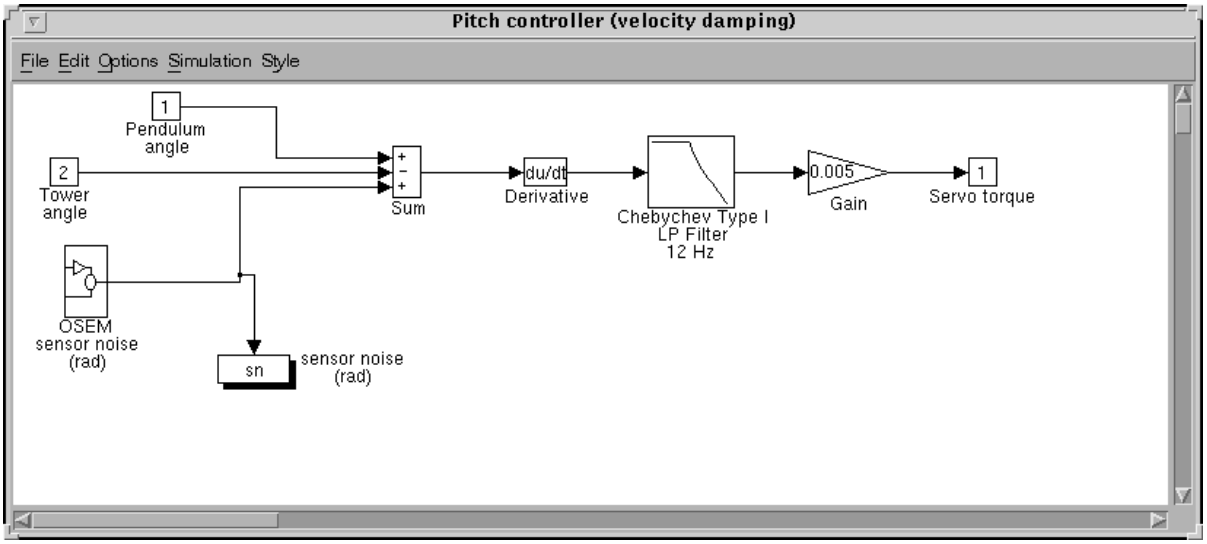

Figure 21: Velocity damping servo (for pitch)

ment, and the residual pitch motion (this is like an open loop and closed loop measurement) We see there that the sensor noise contributes at low and high frequencies, and the pendulum is critically damped at the pitch and pendulum resonances. The pendulum pitch is larger than sensor noise (taken as a tilt reference) between 0.1 and 2 Hz: that means that we could take the suspension tower tilt (plus sensor noise) as reference for a tighter servo and do better than just provide critically damping at resonances.

- The residual rms pitch, over an integration time of 100 second, is 4.5 10^{-7} radians, which just about the requirement to allow lock acquisition (see Ref. 1).

9.2. Modified servo

In order to prove that it is possible to reduce the residual rms pitch motion, if necessary, with a tighter servo, we used a “modified velocity damping servo”, shown in Figure 25 , instead of the velocity damping servo. The servo adds a path with a 2 pole Butterworth bandpass filter between 0.15 and 0.5 Hz, and we use enough gain to tie the pendulum to the tower between 0.1 Hz and 3 Hz. We also eliminated the Chebyschev filter to avoid motion amplification at the cross-over frequencies. The result for the residual pitch motion (again, in Louisiana, with viton spring stacks) using both kind of servos is shown in Figure 26 . The performance of the “modified servo” is limited by sensor noise, but we do obtain an integrated rms level equal to 10^{-7} rad, almost 5 times lower than with just velocity damping. The spectral density is higher at both low and high frequencies, because we trade off the natural pendulum isolation with servo gain tied to a noisy reference (and we have eliminated the low pass filter), but a low spectral density may not be as important as a low rms level in a “lock acquisition” state.

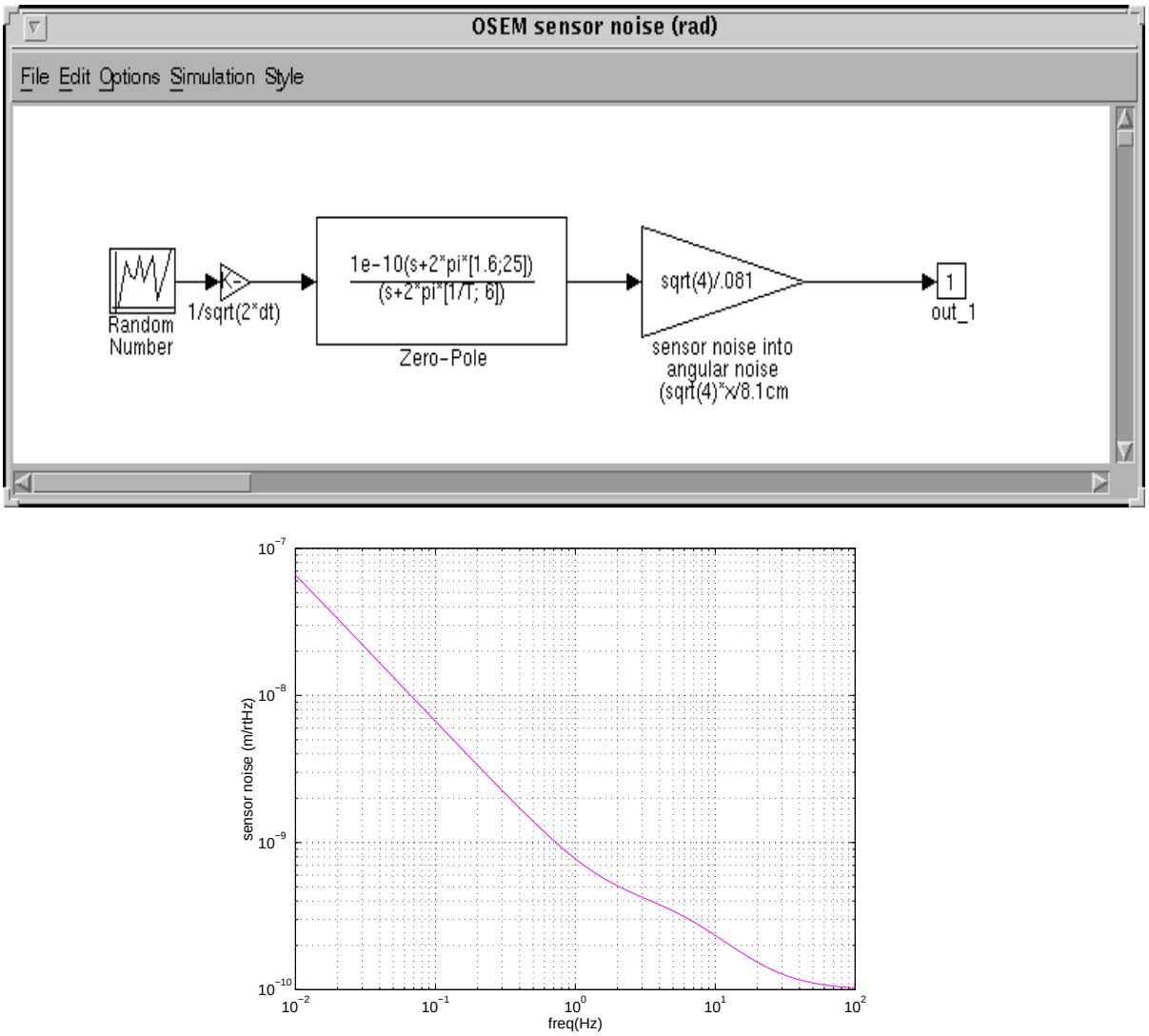

Figure 22: OSEM sensor noise (refer to fig. 3)

9.3. Wavefront sensing servo

We assumed that some of the mirrors will be controlled by wavefront sensing servos to keep the interferometer alignment at the required levels (see Ref. 1). We used the Matlab model for pitch motion to do the conceptual design of such a servo. The block diagram (that substitutes the pitch controller in Figure 3) is shown in Figure 27 . This servo has as input the differential angle between mirrors, in this case, we use just the pitch angle of this mirror (as if we were refer-

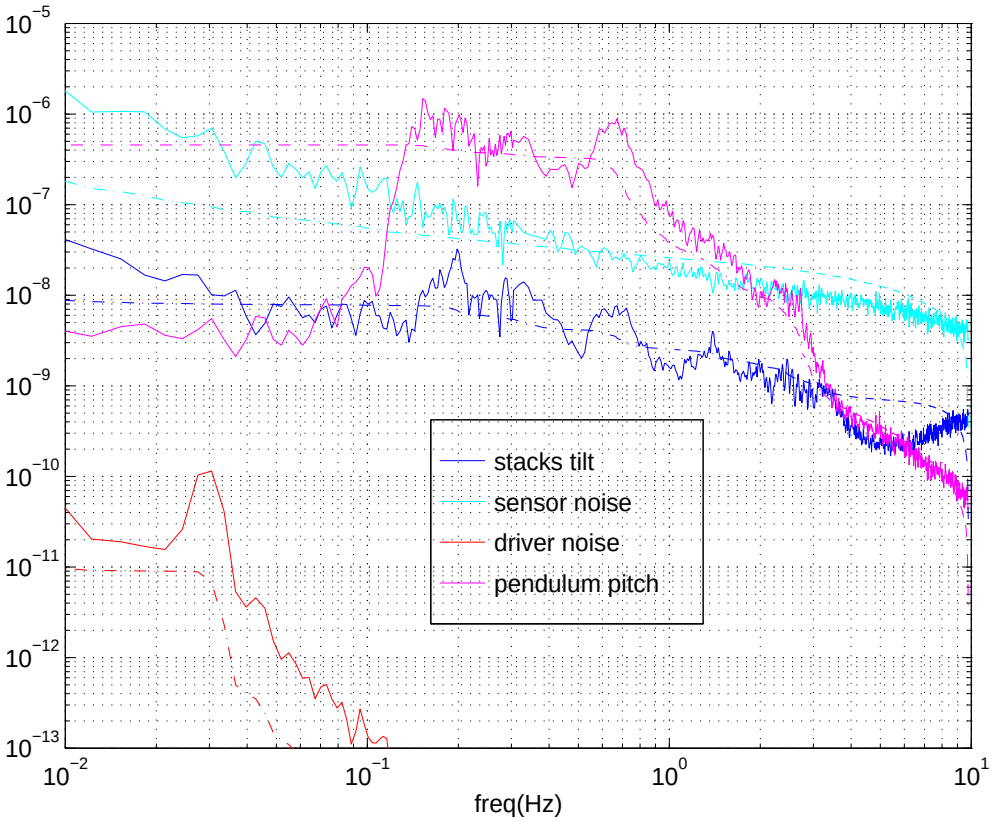

Figure 23: Tilts at different points in the "stacks to pendulum" Simulink block. The solid lines are spectral densities in rad/$\sqrt{\text{Hz}}$ and the dotted lines are integrated rms amplitudes (between *f* and 10 Hz) in radians rms.

encing it to a completely still mirror). The estimated sensor noise is white, at a level of 10^{-15} rad$/\sqrt{\text{Hz}}$. More details about this servo design and results can be found in Ref. 1 .

10 STACKS TO PENDULUMS: RESULTS

10.1. Low frequencies (below 10 Hz)

We present here the results obtained with the "stacks-to-pendulums" Simulink blocks. We have two sites, two different stacks and three servos: that makes 12 simulations. We will present them by site, by servo, with the results for both stacks on the same plot. We will plot spectral den-

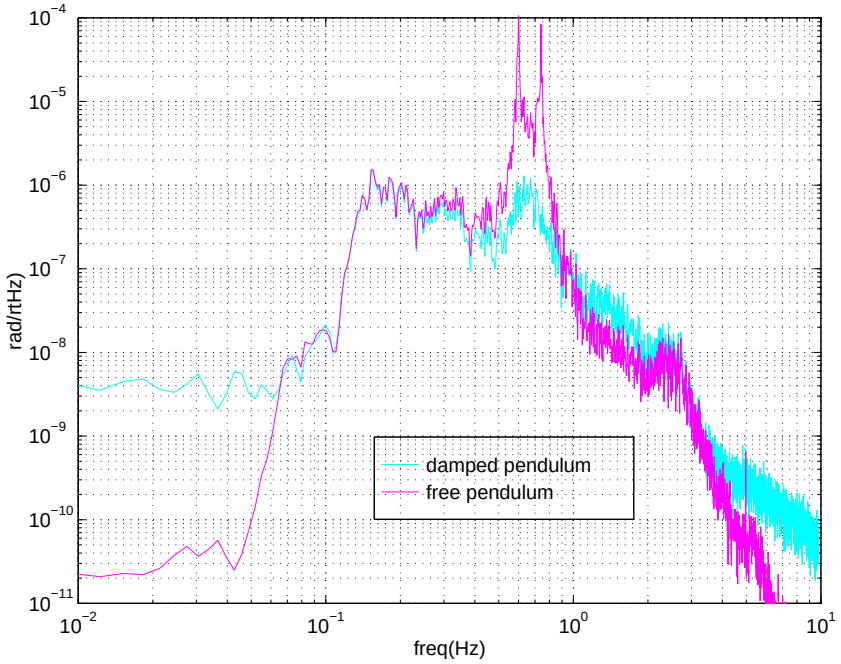

Figure 24: Free and damped pendulum, excited by the suspension tower displacement in Louisiana, with viton spring stacks.

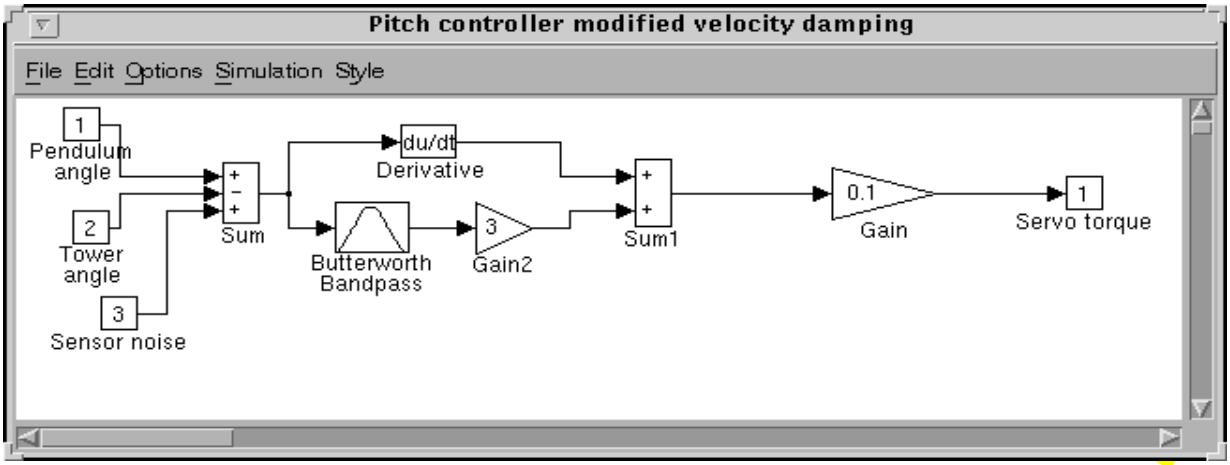

Figure 25: Modified velocity damping servo.

sities of mirror residual pitch angle $\theta(f)$ in rad$/\sqrt{\text{Hz}}$, together with integrated rms amplitudes $\theta_{rms}(f)$ in the band between f and 10 Hz.

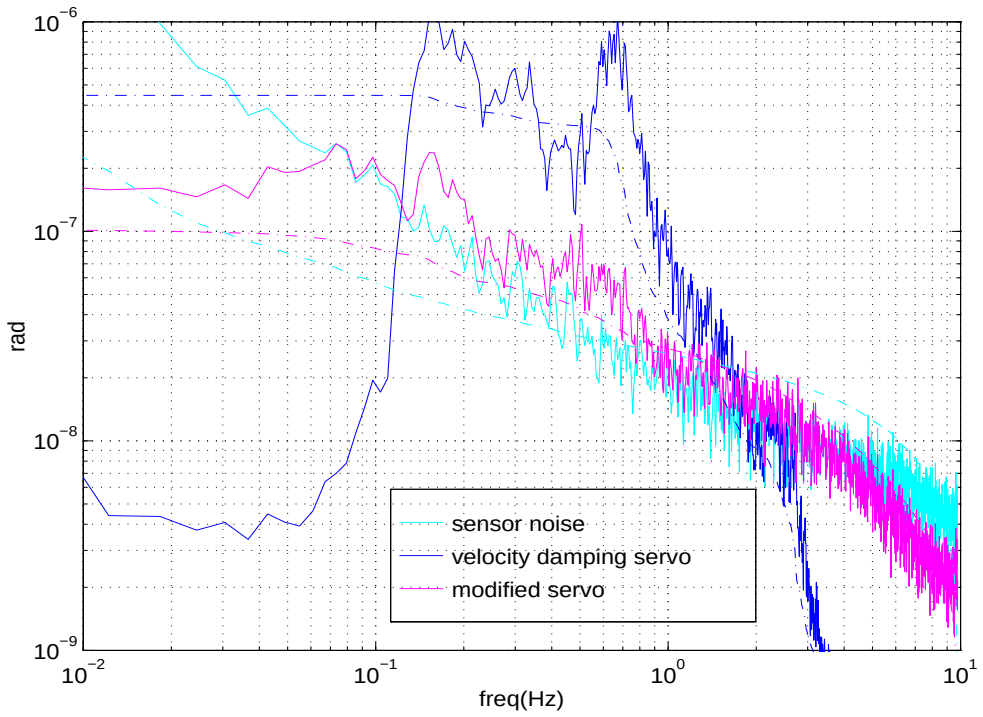

Figure 26: Residual pitch motion for the two local servos considered. The dotted lines are integrated rms motion between *f* and 10 Hz in radians, the solid lines are spectral densities in rad/sqrt(Hz).

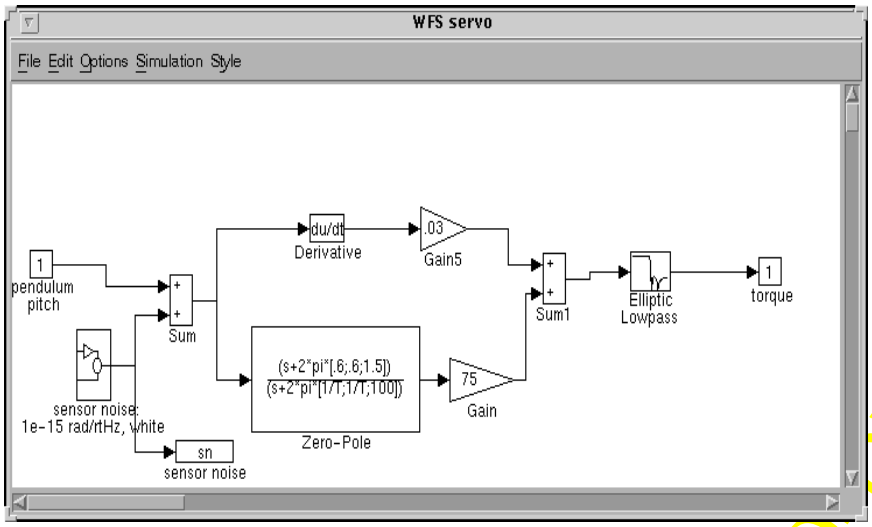

Figure 27: Block diagram for wavefront sensing servo.

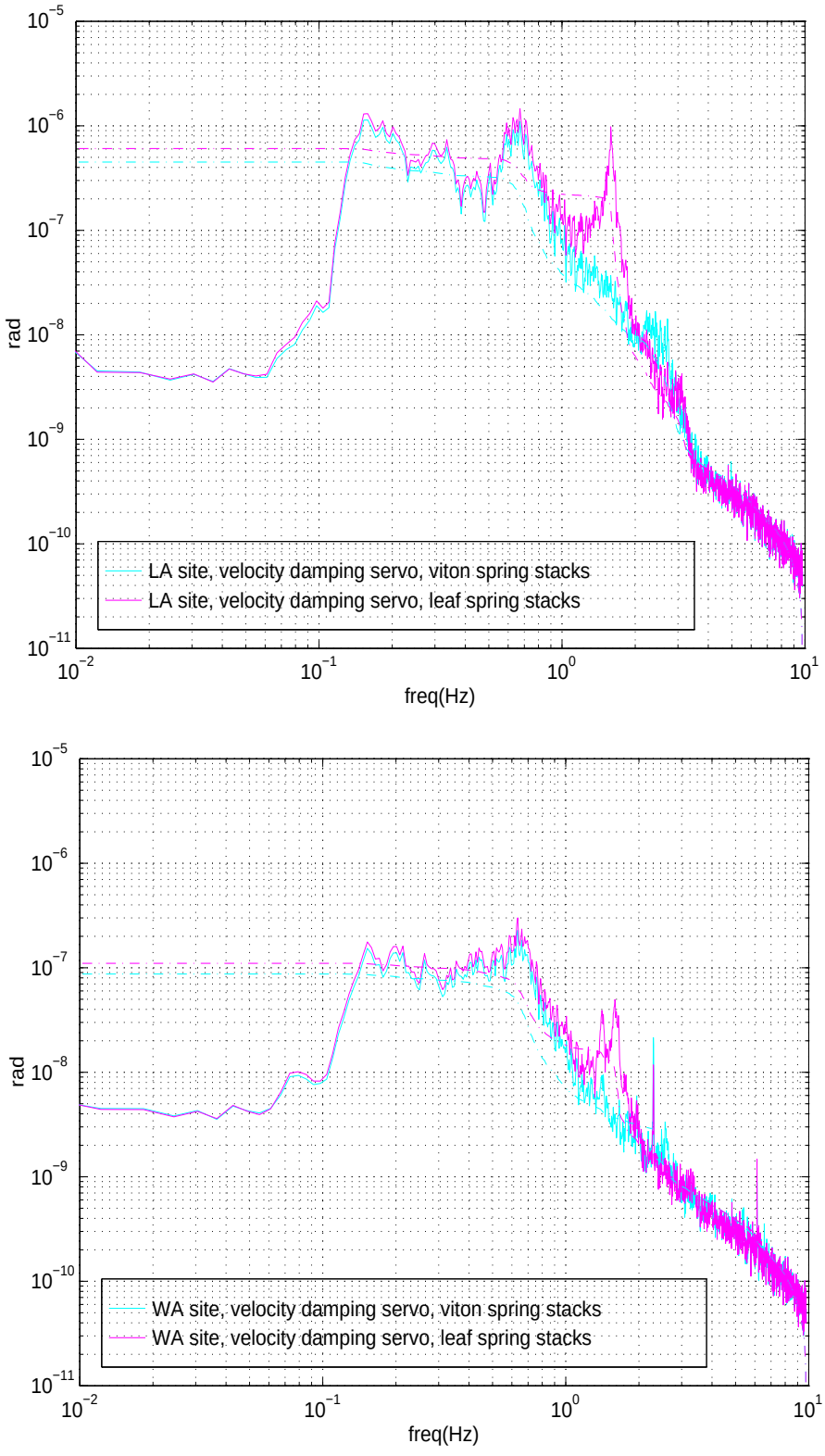

Figure 28: Results for residual pitch angle and velocity damping servo.

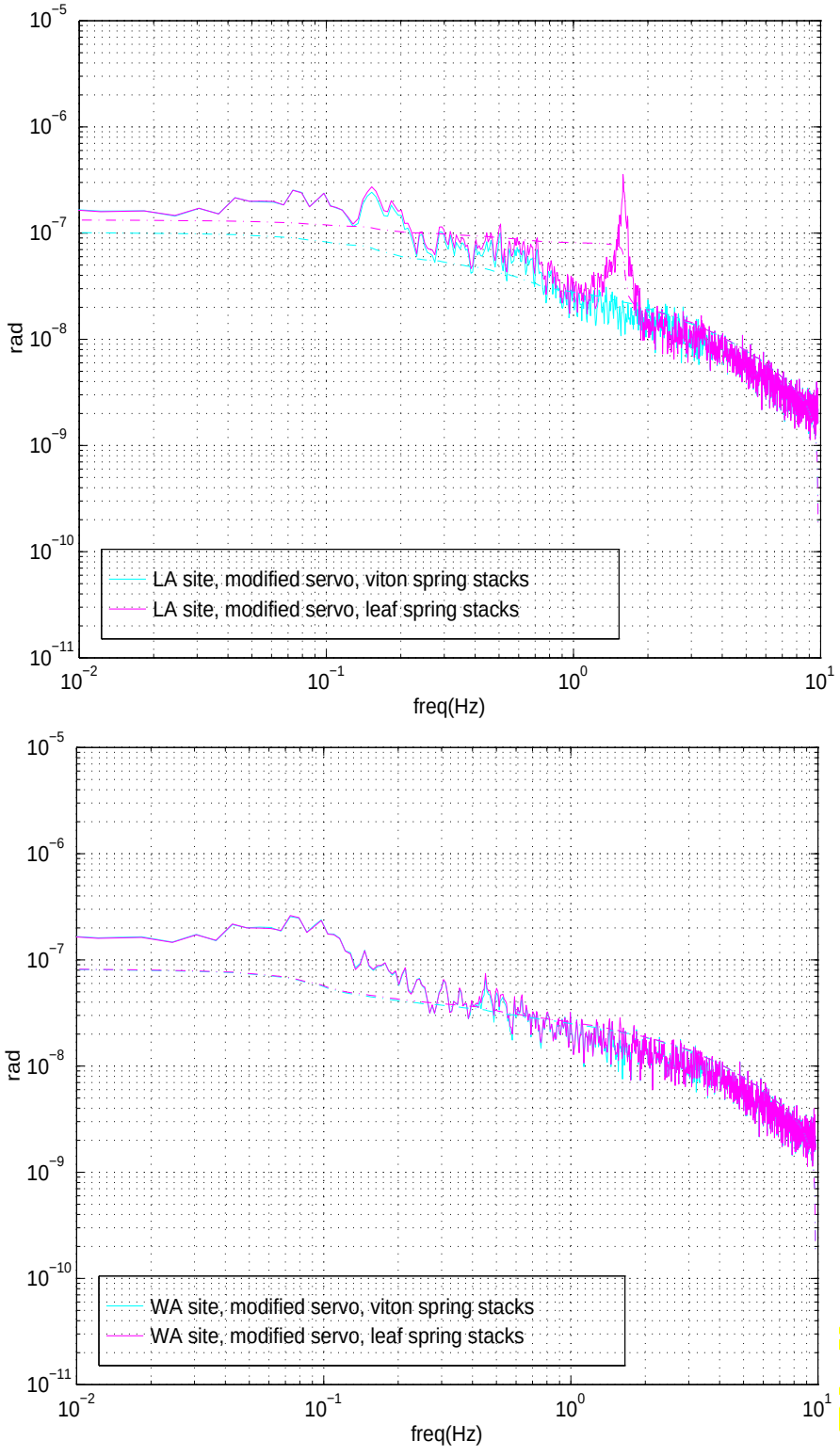

Figure 29: Results for residual pitch angle and modified servo.

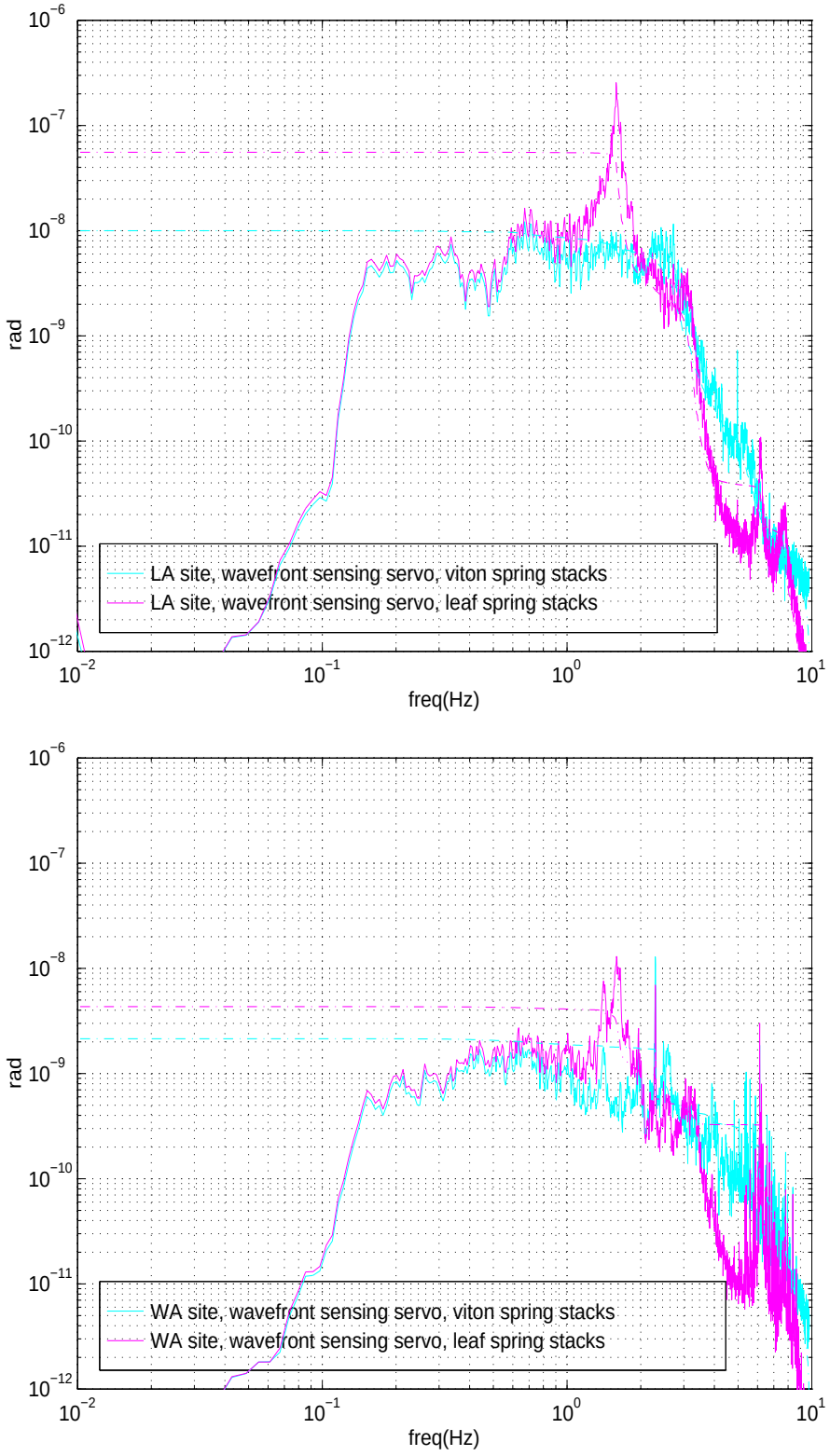

Figure 30: Results for residual pitch angle and wavefront sensing servo.

Next, we present in Table 1 the rms and maximum peak-to-peak (maximum value in the trace minus the minimum value in the trace) values of the results obtained for residual pitch angle:

	velocity damping		modified servo		WFS servo	
	rms	pp	rms	pp	rms	pp
viton spring stacks (LA)	$4.4\ 10^{-7}$	$3.1\ 10^{-6}$	$1.0\ 10^{-7}$	$7.8\ 10^{-7}$	$9.8\ 10^{-9}$	$1.1\ 10^{-7}$
viton spring stacks (WA)	$9.0\ 10^{-8}$	$6.4\ 10^{-7}$	$8.3\ 10^{-8}$	$6.4\ 10^{-7}$	$2.1\ 10^{-9}$	$1.5\ 10^{-8}$
leaf spring stacks (LA)	$5.9\ 10^{-7}$	$4.3\ 10^{-6}$	$1.3\ 10^{-7}$	$1.0\ 10^{-8}$	$5.4\ 10^{-8}$	$4.0\ 10^{-7}$
leaf spring stacks (WA)	$1.1\ 10^{-7}$	$8.2\ 10^{-7}$	$8.3\ 10^{-8}$	$6.4\ 10^{-7}$	$4.2\ 10^{-9}$	$3.1\ 10^{-8}$

Table 1: Rms and peak to peak values of residual pitch angles (in radians).

A few obvious points worth mentioning from the previous results:

Rms and pk-to-pk values:

- The maximum peak to peak residual motion is 4.3 μradians at Livingston, LA for leaf spring stacks and velocity damping servo.
- Rms and peak to peak values at Hanford, WA are smaller than at Livingston, LA by factors of ~5 for velocity damping servos, ~1-2 for modified servo (because it is limited by sensor noise), and ~10 for WFS servos.
- The rms and the maximum peak to peak values are in a ratio of ~1:8-10.

Spectral densities:

- In the velocity damped case, the spectra have their maximum values between the microseismic peak and the pendulum frequency.
- When mirrors are controlled by a modified servo, the spectral shape is dictated by sensor noise, flat at low frequencies, and decreasing above ~1 Hz. The spectra are very similar in both sites in this case.
- When the mirror is controlled with the WFS servo (best case, since it is referenced to an inertial zero with a low noise sensor), spectral densities are ~10^{-8} (LA) or 10^{-9} (WA) $\mathrm{rad}/\sqrt{\mathrm{Hz}}$ between the microseismic peak and ~2 Hz (the high frequency cut off depends on the servo design).
- When the mirror is controlled by the WFS servo, the leaf spring stack resonance is the dominant feature in the spectrum, with an amplitude as high as $3\ 10^{-7}$ (LA) or 10^{-8} $\mathrm{rad}/\sqrt{\mathrm{Hz}}$ (WA) and a width of ~0.5 Hz.

10.2. High frequencies (1-100 Hz)

To study results at high frequencies, we need to do the simulations with sampling frequencies of 250 Hz, but we don't need so long time traces: less than 200 seconds is enough to resolve well below 1 Hz. However, the spectra of most traces decrease very steeply with frequency, and thus the calculation of the spectra from the time trace needs some "whitening" first. We have done the data analysis only for the LA ground noise and the viton stacks, but we think we can draw conclusions for the other cases from this one case.

The main result is the spectrum of the residual pitch motion. The relevant comparisons are with the motion of the "free pendulum", without any controlling servo, and with the pendulum angular thermal noise, that will add incoherently with the driven motion. We show in Figure 31 the results obtained with the three different servos. It is obvious there the trade off involved when

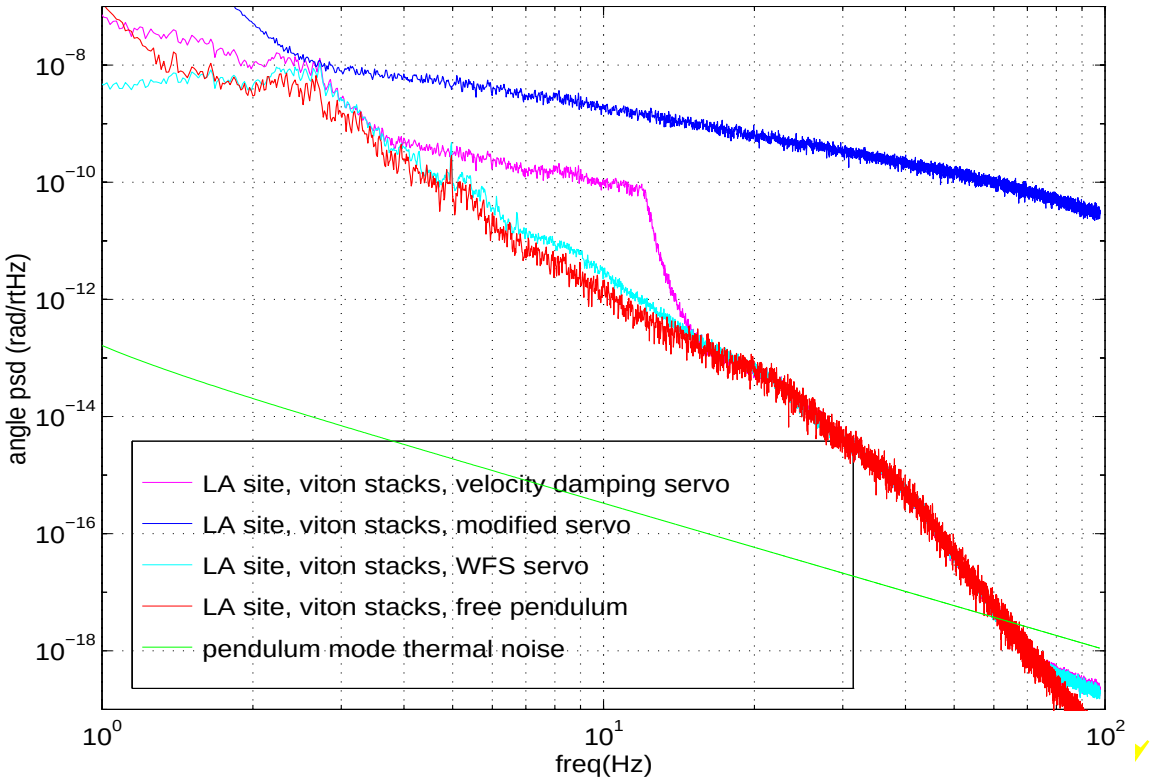

Figure 31: Pendulum pitch spectra for frequencies between 1 Hz and 100 Hz.

tying the pendulum more tightly to the suspension tower (using the "modified servo"): the noise at high frequencies is increased by many orders of magnitude. However, the intention of this servo design was to show that we could obtain a "lock acquisition" baseline, with pendulum pitch rms below 10^{-7} radians, but it was assumed that this servo did not need to fulfill the requirements at higher frequencies, in particular, we eliminated the steep low pass used in the velocity damping servo.

The residual spectrum of pendulum controlled with the velocity damping servo approximates the spectrum of a free pendulum soon after the cut off frequency of the Chebyschev filter. The residual pitch angle when the pendulum is controlled both with the velocity damping servo and with the wavefront sensing servo is above the free pendulum spectrum only above 80 Hz, where the driver noise begins to overtake. However, at those frequencies, the spectrum is below the pendulum thermal noise spectrum, so both servos satisfy the requirement of not adding noise to the thermal noise level.

Notice that the seismically induced motion is larger than thermal noise motion below 60 Hz. This is different than what we assumed in the ASC DRD (Ref. 1) when setting entering requirements. This is because in that case we only considered ground displacements filtered by the stacks as the source of motion, and here we saw that with our assumptions, the building tilts, filtered by the stacks and then transmitted through a lever arm in the downtube, produce larger displacements than just stack displacements.

The leaf spring stacks should improve these spectra, since the stack isolation above resonances is better than with viton spring stacks. However, with the same assumptions, it will still be true than stack tilts produce larger displacements at the suspension points than stack displacements.

11 THINGS I HAVEN'T DONE (YET)

We list here things we would like to do but haven't done yet with respect to mirrors angular noise:

- We haven't calculated the vertical to tilt coupling through the mirrors curvature, but a quick estimate shows that it shouldn't contribute to the residual rms pitch motion.
- We haven't modeled results for mirrors controlled by optical levers.
- We haven't considered the effect of magnetic fields on the suspensions.
- We should have a model for yaw motion. In principle, if yaw motion is just excited by rotations of the optical table, and rotations of the table are comparable to ground shear, yaw motion should be much smaller than pitch. But we know that yaw is also excited by mechanical asymmetries, that coupled to translational noise might be a larger contribution to yaw than the straight coupling.
- We should have experimental validation of the models used here. In principle, we should be able to use the same model with minor modifications applying as input ground noise measured at the MIT lab and predict the motion of the PNI mirrors. In particular, I worry about PNI mirrors not moving less in yaw than in pitch, as we argued in the previous point.
- We think couplings due to asymmetries in pitch motion contribute less than the longitudinal-to-pitch coupling, but this assumption should be better supported.
- Controller cross couplings are straightforward to put in the model, but I haven't yet done it.
- Hytec has just finished more modeling of the stacks, including cross couplings: the assumptions made here should be compared with their modeling, and even better, we should include

their models in the corresponding Matlab blocks.

12 CONCLUSIONS

We have presented here a model that allows us to calculate mirror angular noise in the time domain. Given time traces measured or generated for the different noise inputs (ground noise, electronics noise, etc.), and assumed transfer functions for each stage, we can use a Matlab-Simulink model to generate a time trace for the residual angular noise. The model proved very useful to study the contribution of different inputs at different time scales: drifts can be "compared" with stack resonances and spectral densities at 100 Hz. The simulations do not take much computing time:~few minutes per case. In fact, the analysis of results, computation of spectra and plotting of results may take in the end more time than the actual generation of results.

Summarizing the results obtained for pitch angular noise in the suspensions:,

- The residual rms angle is mostly the integration in the frequency band between the microseismic peak and a few Hz. Stacks resonances might contribute substantially to the rms. The rms of the velocity damped pendulum is 1-6 10^{-7} radians rms, varying with the sites and different stacks.
- The rms value can be reduced servoing the angle to a quiet reference such as the suspension tower tilt, or to the differential alignment measured with wavefront sensing. Limited by sensor noise as modeled, rms values of 10^{-7} radians rms can be obtained. With WFS, rms values can be reduced below 10^{-8} radians rms, if the servo is adapted to the particular stack.
- The servoing to the tower referenced is limited by sensor noise, and it is not a good reference at higher frequencies, so it should be considered a "lock acquisition" servo.
- The spectrum is essentially generated by the displacement the suspension tower. The spectrum has a rather flat top, between 10^{-6} and 10^{-7} $\mathrm{rad}/\sqrt{\mathrm{Hz}}$ in the band between 0.15 Hz and a few Hz. At low frequencies, the spectrum falls steeply until drifts begin to take over, at a few 10^{-9} $\mathrm{rad}/\sqrt{\mathrm{Hz}}$ (although drifts do not contribute to rms angles until at least few hundred seconds); at high frequencies the slope of the spectrum depends on the stacks transfer functions (unless referenced to the tower tilt).
- At high frequencies, the suspension tower displacement might have substantial contributions from stack tilts: the cross over between seismically induced angular noise and thermal noise depends highly on the modeling of the stack tilts. These tilts, in turn, according to the model used here, are mostly due to air pressure fluctuations tilting the building foundation through vacuum loading. These conclusions could change the beam centering requirements adopted in Ref. 1 , which were based on the angular thermal noise spectrum.

13 REFERENCES

1. LIGO T952007-03-D: Alignment Sensing/Control Design requirements Document.
   LIGO T960134-00-D: Alignment Sensing/Control Conceptual Design.
2. C950572-00-O: A. Rohay, Ambient Ground Vibration Measurements at the Hanford, WA

LIGO site.
3. D. A. Agnew, Strainmeters and Tiltmeters, *Rev. of Geophys.*, **24** 579-624, 1986vp
4. LIGO XXX: Parson's preliminary Design Report Presentation, Nov. 9,1995.
5. Dennis Coyne, Rai Weiss, personal communication.
6. E.E. Gossard, Spectra of Atmospheric Scalars, *J. Geophys. Res*. **85**, 3339-3351, 1960.
7. J. Giaime, P. Saha, D. Shoemaker, L. Sievers, A passive vibration isolation stack for LIGO: Design, modeling, and testing, *Rev Sci. Instrum.*, **67** 208, 1996.
8. T960074-05-D S. Kawamura, J. Hazeel, Fred Raab, Suspension Preliminary Design. T950011-14-D S. Kawamura, F. Raab, Suspension Design Requirements.
9. T960040-00D Seiji Kawamura, Response of Pendulum to Motion of Suspension Point.
10. T950072-00-R S. Kawamura, J. Mason, Evaluation of Proposed Changes to the Suspension Sensor Electronics.
11. LIGO TXX, Pendulum Mechanical Cross Couplings, G. Gonzalez, (in preparation).

APPENDIX 1 GROUND TILTS

We want to include here some of the logic and references used in the model for ground tilts. We also compare literature found on ground spectra with the spectra at the sites.

We begin with displacement ground noise. We have measurements of seismic spectra for the horizontal and vertical ground motion at the sites, for frequencies above 0.1 Hz. The dominant contribution to the rms in the 10-sec time scale is the microseismic peak. There is lots of literature about that particular peak, from which we can estimate the tilt and shear at the ground for a particular wave that has the measured horizontal and vertical amplitude. For longer time scales, we can refer to measurements done in other sites by geophysicists, and scale them so that the microseismic peak amplitude corresponds to the measured one (or using some appropriate criterion). There are no measurements of ground shear (that we know about), and measurements of tilts are "corrupted" by cross coupling from horizontal accelerations, so we don't have actual measurements at the sites or anywhere else of tilts and shear, [1]but again we can assume some characteristics of the earth motion (such as wave speed, for example) at different frequencies and then estimate from measurements of accelerations and strains spectra for tilt and shear.

We will assume that at each frequency, the dominant component is a seismic wave with a particular speed: this could be a "body wave" (traveling through the earth body), a "surface wave" (traveling with a wave vector parallel to earth's surface) or some other locally generated wave. There are three kind of waves that can propagate in earth, defined with respect to the local horizontal: P waves (longitudinal waves, producing horizontal displacement and strain), SV waves (transverse waves, producing vertical ground motion and tilts) or SH waves (transverse waves, producing horizontal displacement and shear). In body waves, all three modes are independent; in surface waves, there are two modes: Rayleigh waves, a combination of P and SV with a ratio close to one; and Love waves, just a name for the SH mode. Love waves are solutions to the problem of propagation only if there is a layered surface (the speed of sound is different at different depths), so the ratio of Love waves to Rayleigh waves generated by a common mechanism (like a storm at sea) varies with the place at which they are measured (but not by orders of magnitude, in general).

1. FJ Raab just provided me with some measurements that we haven't included yet in the modeling presented here

There are three different kind of instruments used to investigate the ground motion: seismometers, strainmeters and tiltmeters. Both seismometers and tiltmeters can be thought of as pendulums, and thus they are sensitive to the same accelerations (scaled by the acceleration of gravity). In fact, sometimes a graph for "tilt" is shown in papers where the data is the same as the data taken with a horizontal seismometer, scaled by ω^2/g. To understand what each instrument is measuring, let us assume there is a wave of the form $x_0 e^{i(kx-\omega t)}$, in all three polarizations (with the same frequency and wave number, and same amplitude in each mode). The "true" displacement in all three directions has amplitude x_0, and the "true" tilt and shear are equal to kx_0 (where "true" refers to some inertial frame). If the ratio gk/ω^2 is large, (the wave has a short wavelength and a low frequency), the "pendulum" is not going to move much in the inertial frame because the accelerations are small, but the local frame, using as "vertical" reference the perpendicular to the ground, is going to tilt, producing a measurable horizontal displacement. In a tiltmeter, the true is opposite: when the ratio gk/ω^2 is small (the wave has a long wavelength and a high frequency), we measure accelerations and not true tilts. In general, then, the seismometer output will be $x = x_0(1+gk/\omega^2)$, and a tiltmeter output will be $t = kx_0(1+\omega^2/gk) = x_0\frac{\omega^2}{g}(1+gk/\omega^2)$. We can see that the instruments outputs are simply related by the factor ω^2/g, although neither output measures only true displacement or tilt. (All the formulas for a particular seismometer design are worked out in [Rodgers], but the conclusions are mentioned in many references, in particular in [Agnew], as obvious). Seismometers are also tiltmeters at low frequencies, and tiltmeters are seismometers at high frequencies (!). However, if we wanted to get the true tilt or displacement from any given measurement, we should also know the wave number, which is itself a function of frequency. There is a known, theoretical dispersion formula for each kind of wave, but we will have different waves at different frequencies. Therefore, the "crossover" frequency is not obvious or even well-defined.

Leaving all the caveats apart, if we have a function $k(\omega)$, we can deduce from a seismometer output $x(\omega)$ two spectra: the "true" displacement $x_0(\omega) = x(\omega)(1+gk/\omega^2)^{-1}$ and the "true" tilt (equal to shear), $\theta(\omega) = k(\omega)x_0(\omega)$. The factor gk/ω^2 might have in general a weight different from one and the shear to tilt ratio might also be different from one, depending on the ratio of wave numbers and the ratio of horizontal and vertical displacements; but we will assume all these factors are all contained in the uncertainty of $k(\omega)$.

Strainmeters are completely different devices: they are either "laser strainmeters" (interferometers, some with a baseline of 732m!) or "rod strainmeters". In either case, given our model for the isotropic wave, these instruments would measure $\varepsilon = kx_0$, same as tilt or shear. However, they are not affected by accelerations (they do not need a "vertical" reference). They assume that the wave being measured has a wavelength long compared with the baseline, but that local strains have a short wavelength compared to the same baseline, so they are measuring propagating waves.

If the model is consistent, then the outputs of a seismometer and of a strainmeter should be related by $\frac{\varepsilon}{x} = k(\omega)(1 + gk(\omega)/\omega^2)^{-1}$. Given independent measurements of strainmeters, seismometers and a function $k(\omega)$, we could take this relation as a consistency check.

So, what real data do we have?

At the sites, there are the measured spectra by Alan Rohay. We will use a "fit" by straight lines (in log-log scale) that Lisa Sievers made, shown in Figure 4 and Figure 5 Vertical and horizontal spectra are similar enough that we model them both with the same curve. The spectra are different in LA and WA, and there are "quiet" and "noisy" spectra for the WA site. We will take the noisy spectrum at WA, and keep the spectra for LA and WA separated, since they are sufficiently different. These spectra are only valid above 0.1 Hz, and we would like to get information about lower frequencies.

There is a spectrum of ground motion often mentioned in geophysical papers, taken as a lower bound for the microseismic background. The paper, "Ambient Earth Motion in the Period Range from 0.1 to 2560 sec", by James Fix (from Teledyne Geotech), [Fix], says that "the spectra are representative of the quietest seismograph stations presently known". We take this paper as reference not because the spectrum is low, but because it has data at very low frequencies, it resolves the microseismic peak (and its companion at half the frequency) very well, and it provides tabular data that we could easily type and treat numerically. It is also true that horizontal and vertical spectra are similar, so we took the data from the vertical spectrum. [1]

If we assume that the shape of the spectrum is generic, we can then scale it to the sites' spectra in the overlapping frequencies, and finally extrapolate from that match the low frequency spectrum at the sites. If we wanted to scale Fix's spectrum in this way, we need a factor of 20, which looks suspiciously high at low frequencies. We show these spectra in Figure 32 .

In another paper describing strainmeters and tiltmeters, [Agnew], there is a "range" for strain noise power spectra, from 10^{-7} Hz to 10 Hz. We took a few points and reconstructed the curves for the lower and upper bound curves, between 1 mHz and 10 Hz. We plot in Figure 33 these strain spectra. (The lower curve does not show the microseismic peak because it has been filtered from the data on purpose.)

In the same paper by [Agnew], there is a description of wave speeds at different frequencies: "for frequencies above 0.5 Hz, the sources are body waves with c=10 km/s or more, plus local sources. Between 0.5 Hz and 0.05 Hz, the largest source is microseisms: surface waves generated at sea with c~3 km/sec. For frequencies of 1 mHz to 0.05 Hz, the noise appears to be caused by atmospheric pressure changes deforming the ground. Wind turbulences propagate at the wind velocity, c=5-30 m/s. During calms, the main source of pressure fluctuations is infrasound (c=300m/s)"

We used these numbers and made a "straight lines fit" in log-log scale, shown in Figure 34 . The straight segments are the numbers quoted in the given frequency range, the stars are the points we used to interpolate the curves. We have two curves distinguishing the lowest and highest

1. We have now gotten (thanks to D. Shoemaker) more comprehensive measurements and bounds for ground noise. They look comparable to the ones used here, and will be analyzed in more detail soon.

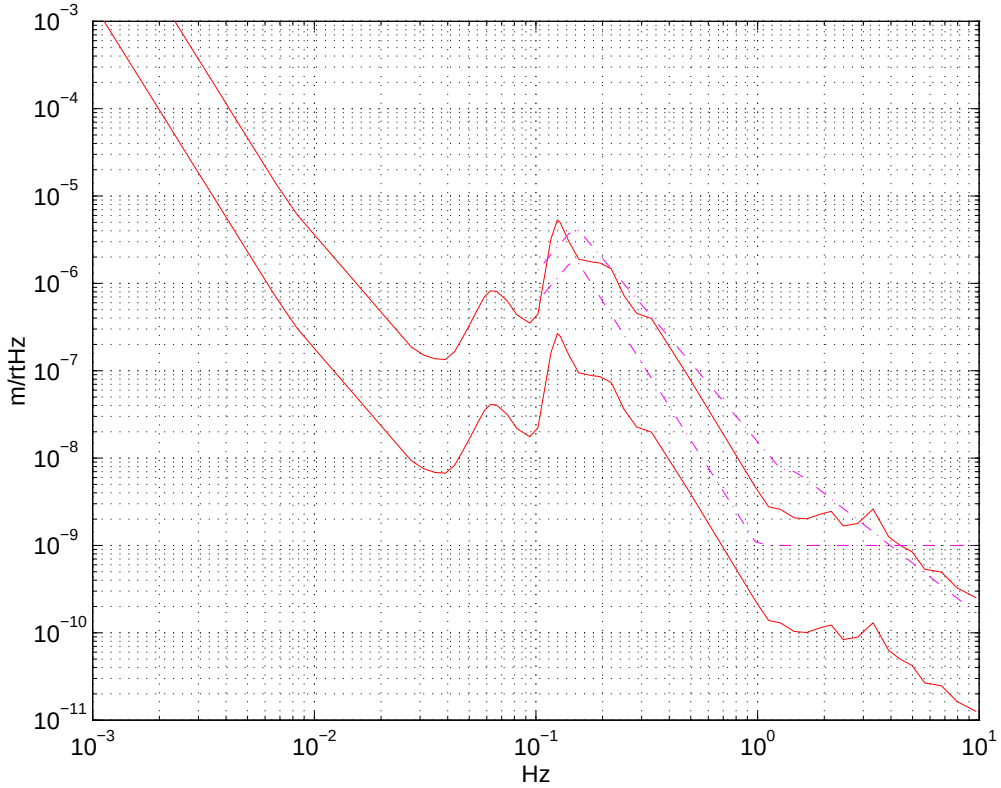

Figure 32: Seismic spectra at the sites and at Queen Creek, AZ (original and scaled by 20)

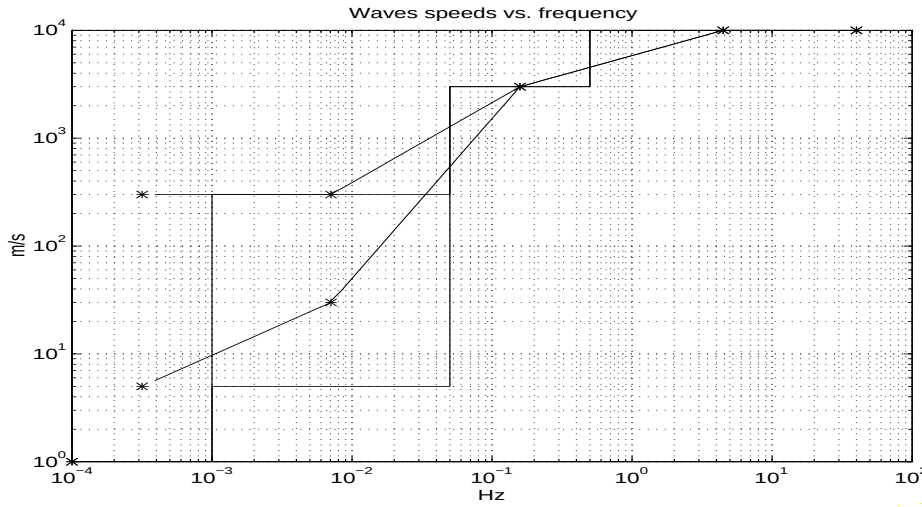

Figure 34: Wave speeds as a function of frequency (from [Agnew])

speed at low frequencies. From the interpolated curve, we can calculate a dispersion relation $k(\omega) = \omega/c$, shown in Figure 35 .

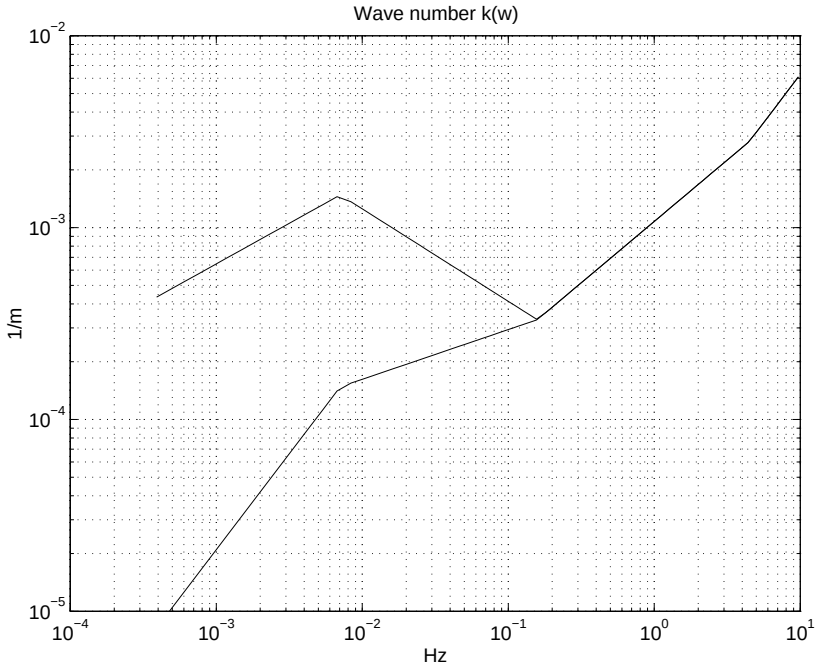

Figure 35: Dispersion relation k(ω), lower curve is due to infrasound, higher one to winds.

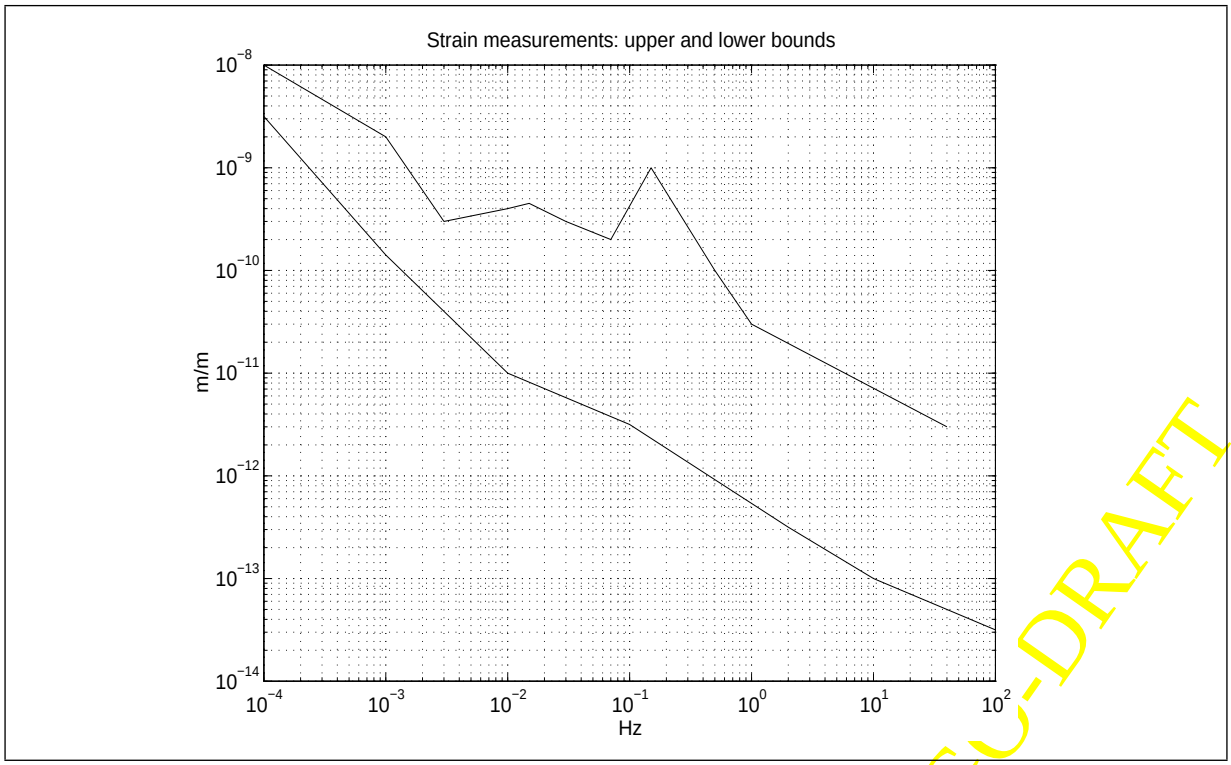

Figure 33: Strain measurements: upper and lower bounds (from [Agnew]).

We can then try out our model (and/or assumptions) converting both strain measurements and seismometer data into “true” displacement, using the function $k(\omega)$ that we have calculated. These curves are shown in Figure 36 . The red curve is from the Queen Creek site, the magenta curves are from measurements at the sites, and the two cyan curves are from the strain measurements. The splits are low frequencies are due to the different estimates for the low frequency wave speeds.

The strain and seismometer measurements are then consistent with the model, or at least as far from the model as the seismometer data are from each other. It may be funny (or sad) to notice that the spectrum at the LA site coincides with the *upper* bound from strains, while the Queen Creek spectrum is consistent with the lower bound of strains.

We take this plot as a validation of the model, up to at worst an order of magnitude but probably better. Thus, we will assume that we can estimate the spectra of displacement, tilt and shear at the sites applying the appropriate formula to the seismometer data (and assuming $k(\omega)$ as shown). Notice, however, that Fix’s spectrum at low frequencies goes from the lower bound to the upper bound, which might indicate some corruption of the measurement at low frequencies.

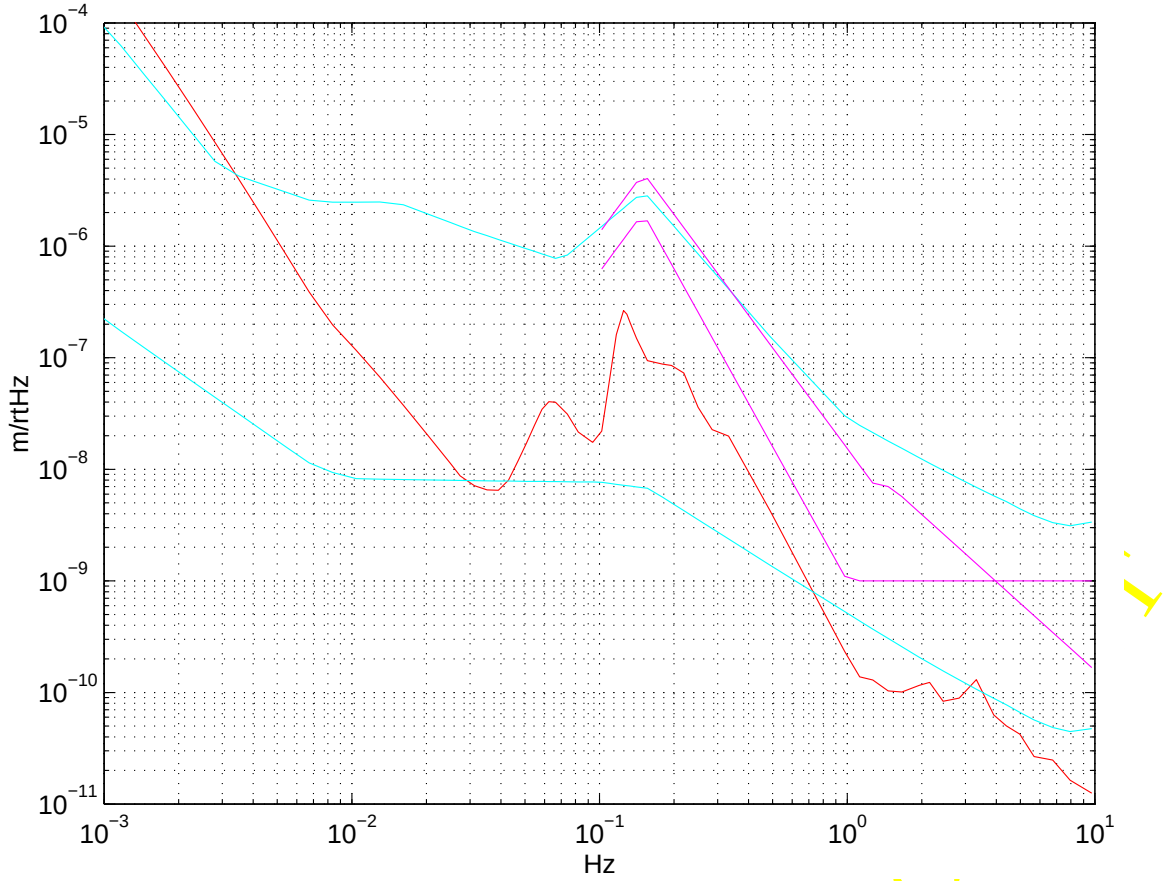

Figure 36: Displacement noise in an inertial frame at the sites, at Queen Creek, AZ and derived from strain upper and lower bounds.

To get the data (or at least a bound for it) at low frequencies, we will scale the Queen Creek spectrum by a factor of 20, that puts in the middle of the curves of WA and LA. We plot in Figure 37 and Figure 38 the spectra for the “true” displacements and tilts, as well as the rms amplitude added as a function of frequency. In symbols, if $x(f)$ is the spectrum in m/rtHz, then we define $x_{rms}(f) = \sqrt{\int_f^{f_{mx}} x^2(f)df}$.

Notice that the rms displacement for 1000 sec according to this scaling is more than 1 mm, while it is 77 microns in the original measurement by Fix. We expect the original measurement (without any scaling) to be more realistic even at the sites. The rms for times shorter than 100 seconds is 1 micron, and this is a reasonable number that agrees with the measured value at the sites. Thus, even if the actual rms values for long times is an overestimate, we can consider the corner frequency of 7 mHz below which the rms departs from the microseismic peak, as a lower bound to the actual corner frequency at the sites.

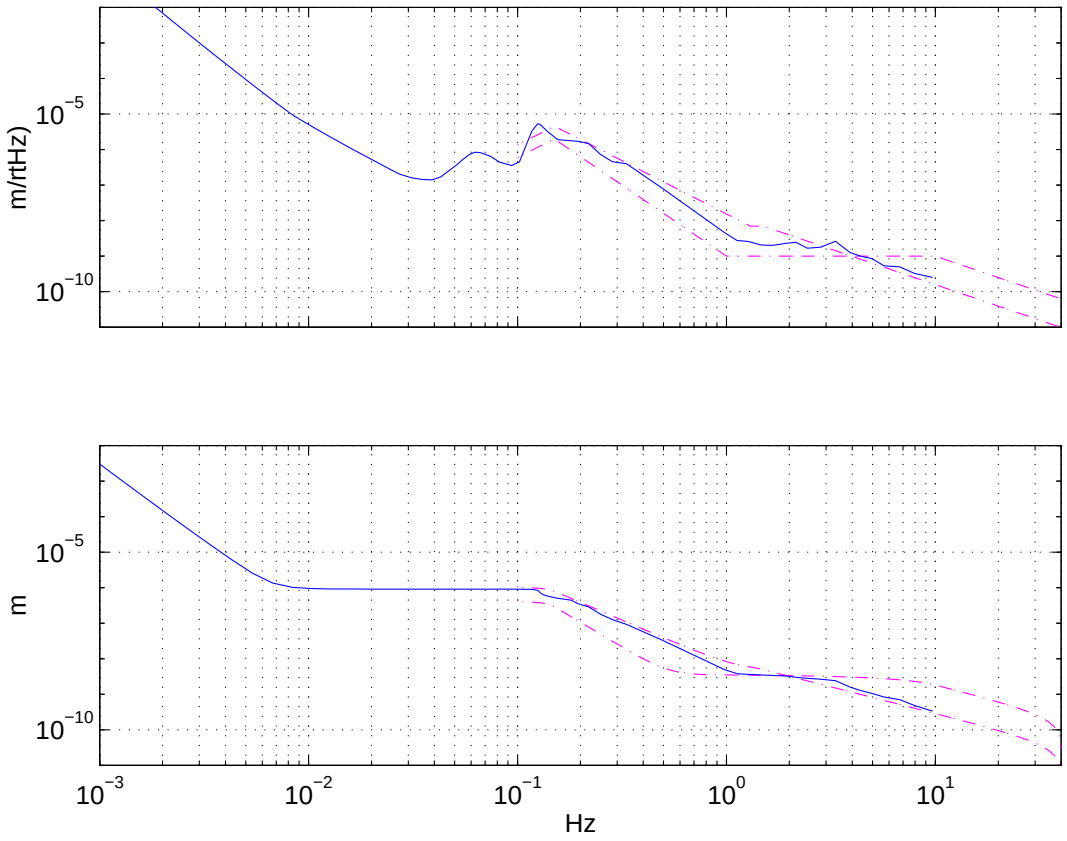

Figure 37: Displacement spectrum and integrated rms, from measurements at the sites and scaled from [Fix] measurements (with a factor of 20)

The spectrum and integrated rms for tilts (and shears, assumed to be the same) is shown in Figure 38 . Again, the rms contributed by the microseismic peak, 0.3 nanoradians, is the dominant contribution until at least times of 500 sec, if the scaling by 20 of Fix's spectrum is right. The spectral density given by the upscaled Fix's spectrum at 1 mHz is 0.1 microradian/rtHz, but we can expect this to be an upper bound more than an estimate. Again, the important information we can take from this is that the corner frequency below which the rms tilt increases over the 10-sec time rms, is not higher than a few mHz.

Data for rms and peak-to-peak ground spectra are presented in section 4 of this document. Since we haven't considered in this modeling effort integration times longer than 100 seconds, we didn't use the Fix spectrum to interpolate data ay lower frequencies; we assumed that the spectrum at low frequencies was low enough that it did not add to the rms value obtained with a 100 seconds integration time.

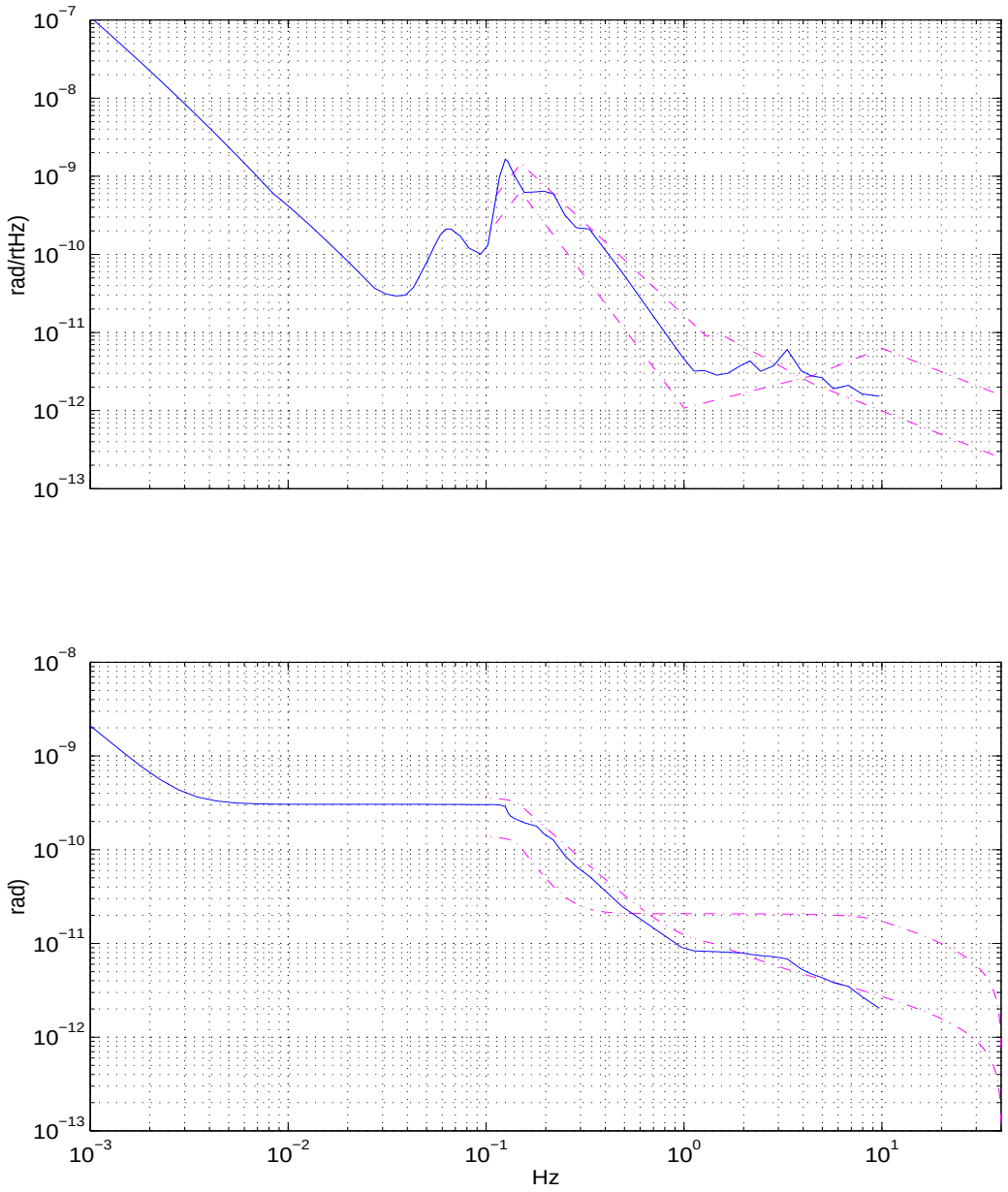

Figure 38: Tilt (and shear) spectrum and integrated rms derived from measurements at the sites and [Fix] spectrum multiplied by 20.

References:

[Agnew]: D. A. Agnew, Strainmeters and Tiltmeters, *Rev. of Geophys.*, **24** 579-624, 1986.

[Fix]: J. E. Fix, Ambient Earth motion in the period range from 0.1 to 2560 sec, *Bull. Seism. Soc. Am.*, **62,** 1753-1760, 1972.

[Rodgers]: P. W. Rodgers, The response of the Horizontal Pendulum seismometer to rayleigh and Love waves, tilt, and free oscillations of the Earth. *Bull. Seism. Soc. Am.*, **58,** 1384-1406, 1968.